AN EXPERIMENTAL STUDY OF

INERTIAL WAVE PROPAGATION

IN A ROTATING LIQUID CONE

by

RICHARD MICHAEL CARTER

A.B., Northeastern University

Submitted in partial fulfillment
of the requirements for the
degree of Master of Science
at the

Massachusetts Institute of Technology

January 1969

Signature of Author
_____
Department of Geology and
Geophysics, January 1969

Certified by
_____
Thesis Supervisor

Accepted by
_____
Chairman, Departmental Committee
on Graduate Students

TABLE OF CONTENTS

ABSTRACT

This paper is a study of inertial wave propagation in
a rotating right circular cone. The energy is supplied to
the fluid by means of a small amplitude harmonic perturba-
tion of the cone. The subsequent exchange of fluid between
the boundary layers and the interior flow is sufficient to
set the fluid into oscillation.

The response of the fluid, as determined with axially
mounted pressure and thermistor probes, and also visually,
was studied as the basic turntable rotation rate was varied.
It was found to be characterized by a series of peaks and
valleys, with the peaks corresponding to points of maximum
response (not resonances). The results were in good agree-
ment with the calculations made using the ray theory of
characteristic refections in a two dimensional wedge. In
an effort to induce resonances in the cone, the bottom
vertex geometry was altered so that the cone now simulated
a frustrum. The response curve revealed an extra peak due
to return reflection of energy, which clearly illustrated
the fact that standing waves could be set up in the cone
with the bottom vertex (a mathematical singular point)
altered.

RANGE OF EXPERIMENTAL PARAMETERS

Parameter	Range

Turntable period, T_T $1.20 \le T_T \le 5.90$ sec.

Turntable frequency, f_T $0.16 \le f_T \le 0.83$ cps

Turntable rotation speed, Ω_T $1.00 \le \Omega_T \le 5.21$ rad./sec.

Cone oscillation period, T_{osc} $T_{osc} = 2.82 \pm .01$ sec.

Cone oscillation frequency, f_{osc} $f_{osc} = 0.355$ cps

Cone oscillation speed, ω_{osc} $\omega_{osc} = 2.22$ rad./sec.

Cone apex half angle $24.16 \pm .15^{\circ}$

Cone base angle $65.84 \pm .15^{\circ}$

Cone height $20.17 \pm .02$ cm.

Cone radius $9.05 \pm .07$ cm.

Cone volume ~ 1723 cm^3.

Oscillation freq/twice rotation speed, $\frac{\omega}{2\Omega}$ $0.213 < \frac{\omega}{2\Omega} < 1.11$

Angle of energy propagation, $\theta = \cos^{-1}\left(\frac{\omega}{2\Omega}\right)$ $0^{\circ} \le \theta < 78^{\circ}$

Cone oscillation angles (peak to peak) $\Delta\theta_{PP} = 18.7 \pm .3, 31.0 \pm 0.3^{\circ}$

Axial heights of thermistor probe $5.13 \pm .02, 10.59 \pm .02$,

                                              $\& \; 15.50 \pm .02$ cm.

Axial heights of pressure probe $10.59 \pm .02$ cm.

Rossby numbers, ϵ_{18}, ϵ_{31} $.03 < \epsilon_{18} < 0.18$

                                             $.06 < \epsilon_{31} < 0.30$

Ekman number, E $0.47 \times 10^{-4} \le E < 2.4 \times 10^{-4}$

1. Introduction

Greenspan (1969) discusses the mathematical problem of flow in a two dimensional wedge and illustrates that this problem exhibits many singular properties to which theoretical answers will not soon appear. An extension from the wedge shape to a three dimensional cone geometry is straightforward. It is the objective of this paper to investigate experimentally the flow inside a rotating right circular cone in an effort to substantiate the findings presented in Greenspan's paper. Before going into some of the features of its interior motion, I will first discuss some conclusions of inertial wave theory in an unbounded fluid which will be of relevance to the cone.

Assuming plane wave solutions of the form

$$(1\text{-}1) \qquad \tilde{q} = Re\left(\tilde{Q}\, e^{i(\tilde{k}\cdot\tilde{r} - \omega t)}\right)$$

$$(1\text{-}2) \qquad p = Re\left(\Phi\, e^{i(\tilde{k}\cdot\tilde{r} - \omega t)}\right)$$

and using the linear equations of mass and momentum conservation (dimensional form) for an inviscid, homogeneous fluid, namely,

$$(1\text{-}3) \qquad \nabla \cdot \tilde{q} = 0$$

$$(1\text{-}4) \qquad \frac{\partial \tilde{q}}{\partial t} + 2\tilde{\Omega} \times \tilde{q} = -\frac{1}{\rho_0}\nabla p$$

where $\tilde{q}$ is the particle velocity measured in the rotating coordinate system of constant angular velocity $\tilde{\Omega}\left(=\Omega\hat{z}\right)$, p is the reduced pressure (Batchelor 1967), $\tilde{k}$ is the wave number vector, ω the frequency, and $\tilde{Q}$, Φ are constants not necessarily real, we can derive the following four relations. From the continuity

equation we obtain

(1-5) $$\tilde{k} \cdot \tilde{Q} = 0$$

which expresses the fact that the waves are transverse. Consider an orthogonal co-ordinate system with the wave number vector $\tilde{k}$ along the $\tilde{c}$-axis, figure 1, and let $\tilde{Q} = U\hat{a} + V\hat{b}$ since from continuity $\tilde{q} \perp \tilde{k}$, then from the momentum equation we obtain the dispersion relation

(1-6) $$\omega = \pm 2\Omega \cos\theta$$

and (1-7) $$\tilde{q} = U\left(\cos\psi\,\hat{a} + \cos\left(\psi \pm \tfrac{\pi}{2}\right)\hat{b}\right), \quad \psi = kc - \omega t$$

Equation 1-7 determines that the particle motion is circular and counterclockwise for choice of the negative sign, or circular and clockwise for choice of the positive sign, figure 2. In a two dimensional X-Z space with the wave number vector as illustrated in figure 3, and recalling that the group velocity $\tilde{C}_g = \frac{\partial \omega}{\partial k_i}\hat{\ell}_i$, where $\hat{\ell}_i$ is a unit vector in the i-direction we obtain the relation

(1-8) $$\tilde{C}_g \cdot \tilde{k} = 0$$

which reveals that the angle between the direction of energy propagation (characteristics) and the wave number vector is always 90°.

One feature of inertial waves is their anisotropic property. The incoming and reflected flux vectors make equal angles with the $\tilde{\Omega}$-axis, and not with the normal to the wall at the point of their intersection as would a non-dispersive wave
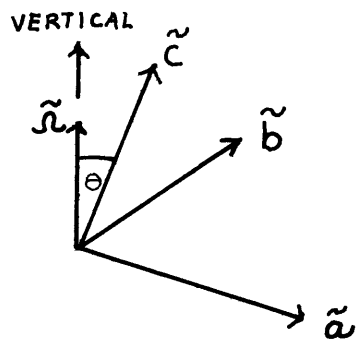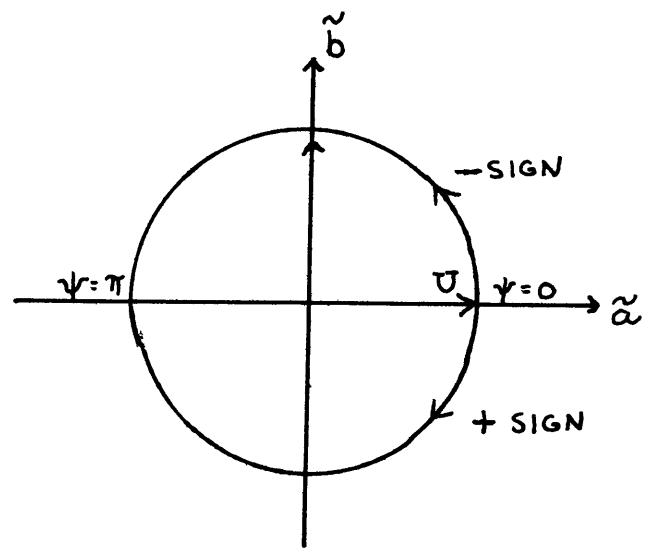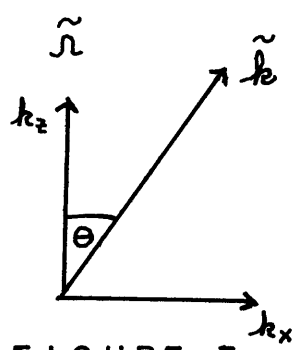
FIGURE 1

FIGURE 2

FIGURE 3

(Phillips 1963). This implies a preferred direction of energy
propagation. Figure 4 illustrates the preferred direction for
the group velocity vector $\tilde{C}_g$; reflection does not obey the equal
angle rule (Snell's law) but rather occurs in a direction from
the vertical given by the dispersion relation

$$\omega = \pm 2\Omega \cos\theta$$

or (1-9)

$$\theta = \cos^{-1}\left(\frac{\omega}{2\Omega}\right)$$

In the cone study, ω, the cone oscillation frequency is a constant,
while $\tilde{\Omega}$, the turntable rotation speed is prescribed for each ex-
perimental run, hence $\left(\frac{\omega}{2\Omega}\right)$ is a constant for each run.

The experimental apparatus consists of a right circular
cone mounted on a precision turntable which rotates with a con-
stant angular velocity $\tilde{\Omega}\left(=\Omega\hat{z}\right)$. Superimposed on this basic
turntable rotation speed is an oscillatory motion of frequency ω
about the vertical $\hat{z}$ - axis such that the overall motion can be
expressed as $\dot{\theta} = \Omega + \frac{\Delta\theta}{2}\omega\cos\omega t$ with $\frac{\Delta\theta}{2}$ equal to the oscillation
angle in radians. It is through the mechanism of this oscilla-
tion that energy is supplied to the enclosed fluid in the form
of inertial waves; the response of the fluid being studied as $\tilde{\Omega}$
is varied. Ekman boundary layers are set up along the top and
side walls of the cone with a type of convergence zone at the
upper corner. The exchange of fluid from this convergence zone
with the interior (separation of flow from the corner) is suf-
ficient to produce oscillatory motion in the cone. The direc-
tion of motion or energy propagation from the corner can be
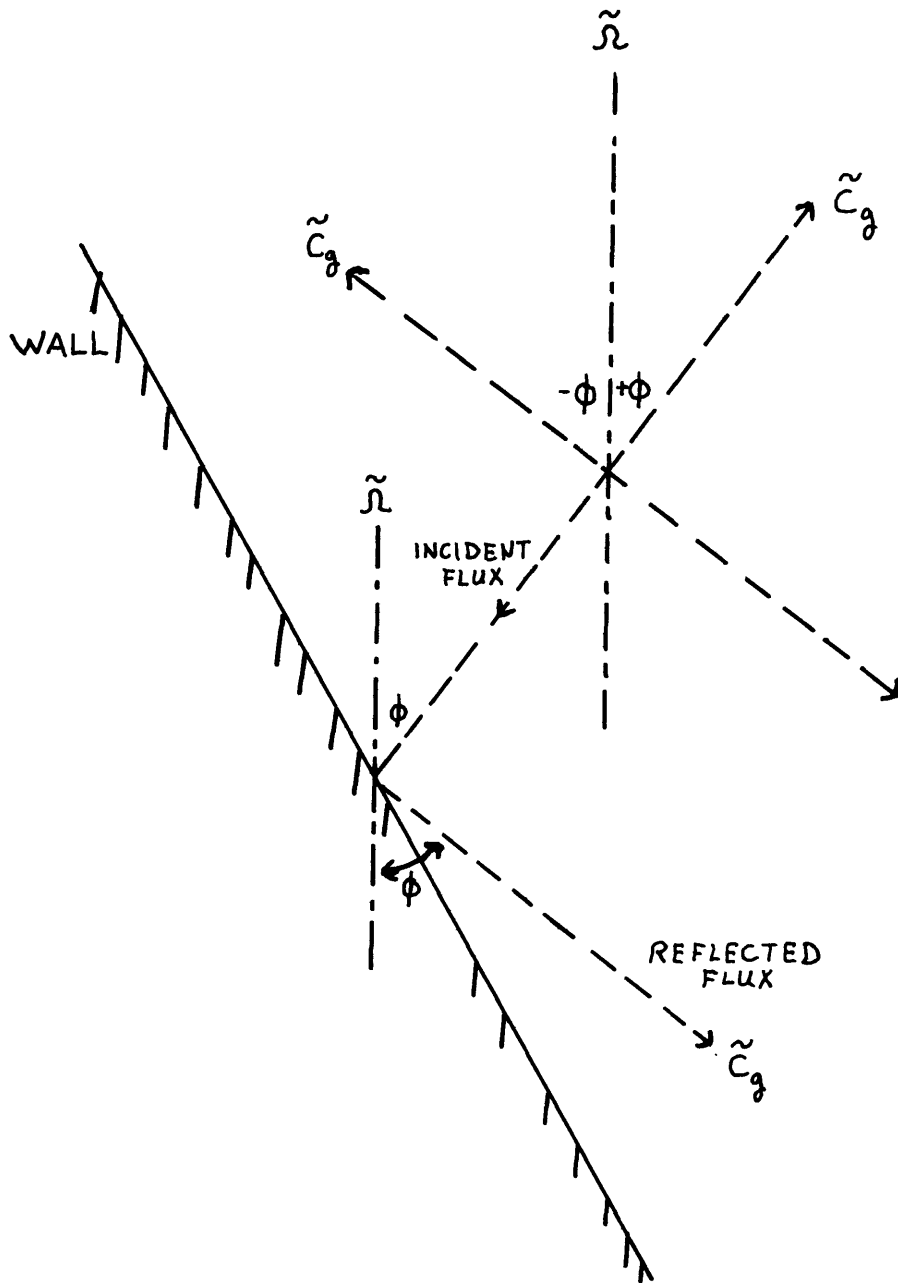
FIGURE 4

described accurately with the dispersion relation $\Theta = \cos^{-1}\left(\frac{\omega}{2\Omega}\right)$, Θ being an angle measured from the horizontal.

As discussed previously these inertial waves will then reflect from the container walls in such a manner that the angle between the direction of energy propagation and the rotation axis remains a constant. The import of this statement is that a packet of energy emanating from the upper corner of the cone must always proceed toward the vertex immaterial of the initial angle of the characteristics. One would suspect that a large quantity of energy would accumulate in the vertex and subsequent return reflection would occur producing standing waves inside the cone. But in fact this does not occur. It can be shown that it takes an infinite time for a wave packet to reach the vertex, the container seems open or unbounded to the interior motion and energy is absorbed with no reflections.

It is interesting to note here that a similar arrangement was used by Aldridge and Toomre (1968) to excite inertial modes in an oscillating sphere. The flux from the Ekman layers along the spherical walls induced resonances at critical rotation frequencies.

It is felt that although there are no resonances in the cone, i.e. the spectrum of inertial waves is a continuous set rather than a discreet one, there will be regions of peak response when the energy in the inertial waves directly excite a measuring device. The sections which follow are successful

attempts at investigating various facets of the interior motion with a thermistor bead and a pressure transducer, both being positioned at specified heights along the vertical axis since the flow is axisymmetric. A later section examines the horizontal structure of the particle motion visually using aluminum flakes and streak photography.

If we were shown a response curve from one of these axially mounted probes we would expect to see a series of peaks and valleys on the curve with the peaks corresponding to places where the energy flux had crossed the center axis at a probe height. The peaks would be of different amplitudes depending on how many energy reflections from the side wall had occurred before it reached the measuring device. One would also suspect that the fluid-particle phase would be altered near the characteristics and this effect might be uncovered with a phase-sensitive detector. Figure 5 is a plot of the axial crossing points of the characteristics in the cone as obtained from equation B-4 of Appendix B. The computer program to obtain these curves is given in appendix C. The curve labeled $m = 1$ gives the axial crossing points for energy propagation directly from the upper corner of the cone. The $m = 2$ curve refers to energy arrival at the axis after having reflected once from the side wall. The $m = 3$ curve represents the energy arrival from the corner after two side wall reflections. And the $m = 4$ curve is for three inertial wave reflections off the side walls before reaching
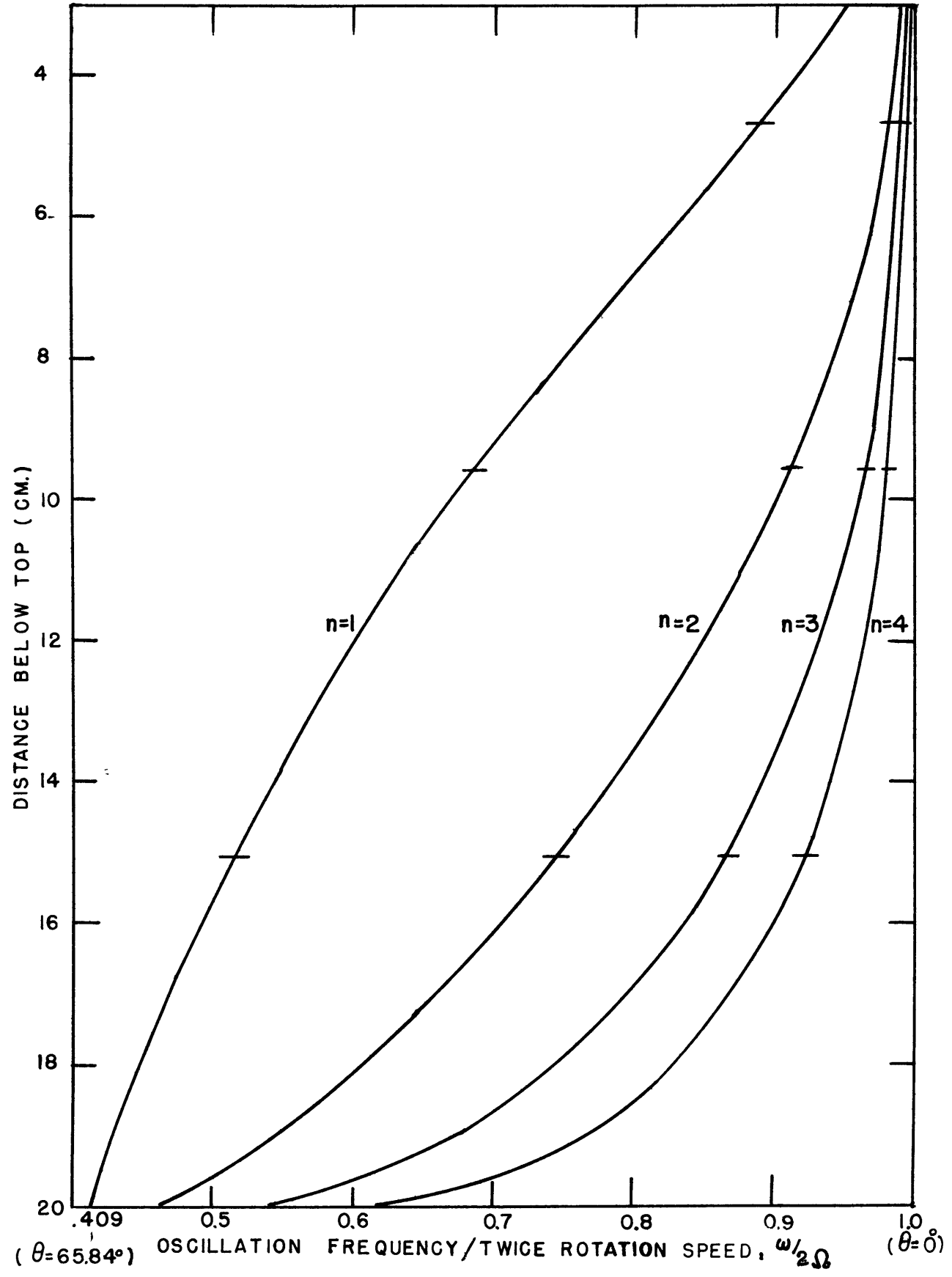
AXIAL CROSSING POINTS OF CHARACTERISTICS

FIGURE 5

the axially positioned sensing device. The reflection of char-
acteristics in a cone is discussed at length in appendix B.
The cross-hatch marks on the curves indicate the depths at which
probes were positioned along the axis of the cone. In general
for any prescribed axial position below the top one can read
the values of the quantity $\left(\frac{\omega}{2\Omega}\right)$ from the curves and then
calculate Ω , the turntable rotation speed necessary to cause
the energy flux to pass through that point.

2. Thermistor Study

a. Apparatus and Experimental Procedure

Thermistor resistance is a function of temperature, the higher the temperature of the thermistor, the lower is its resistance. The heat that the thermistor dissipates can be described adequately by a quantity called its ohmic loss which is the power ($I^2 R_T$ in watts) developed by the thermistor. The circuit design employed in the thermistor study is the simple Wheatstone bridge illustrated in figure 6. The purpose of the $10K\Omega$ potentiometer is to keep normal current in the circuit at a constant value of 12.5 milli-amperes. R_1, R_2, and R_3, are resistors of equal value differing only slightly from the value of R_T, the thermistor resistance. The object of using this bridge is to allow for greater accuracy with considerable ease in the measurement process, accomplishing this by the nulling together of two signals.

Consider the circuit of figure 7.

$$\ell_3 = \frac{\ell_0}{2} \qquad \ell_1 = \frac{\ell_0}{1 + R_T/R}$$

if we choose $R_T \approx R$ then $\ell_1 \approx \ell_3$

let us suppose

$$R = R + \left(\frac{\partial R}{\partial T} \delta T\right) \text{ with the term } \frac{\partial R}{\partial T} \delta T \text{ small}$$

then

$$\frac{R_T}{R} = 1 + \frac{1}{R} \frac{\partial R}{\partial T} \delta T = 1 + \alpha \delta T$$

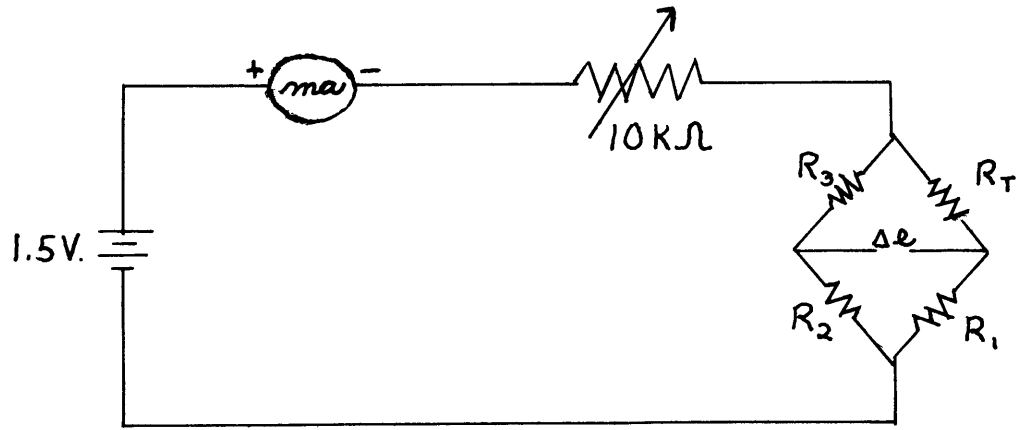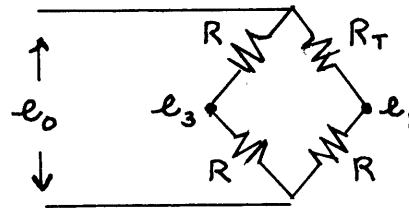where α is the thermal coefficient

FIGURE 6

FIGURE 7

hence $\quad \ell_1 = \ell_0 \left(\frac{1}{2 + \alpha \delta T} \right) = \frac{\ell_0}{2} \left(1 - \frac{1}{2} \alpha \delta T + \frac{\alpha^2}{4} \overline{\delta T}^2 - \cdots \right)$

or $\quad \Delta \ell = \ell_3 - \ell_1 = \frac{\ell_0}{4} \alpha \delta T$

As applies to the thermistor studies, $\Delta \ell$ is the input to a Varian X - Y recorder model F-80A, and according to the above discussion, should be proportional to δT of the thermistor. Hence one can see that as the temperature of the thermistor varies due to the oscillating vertical velocity past the probe, this will be recorded as a voltage , $\Delta \ell$, on the X - Y recorder.

The Veco (Victory Engineering Corporation) part number 21A2 bead thermistor used in the experiment is a small elliptical body of diameter .043 inch, and is made from metal oxide semi-conductor materials, with sintered on platinum-iridium lead wires of .004 inch diameter. The zero power resistance at 25°C is 100 ohms, with an approximate temperature coefficient $\alpha = - 3.2 \%/^\circ C$

The thermistor is positioned in the rotating frame at three specified heights along the vertical axis of the cone. It is connected to an electrical circuit in the non-rotating frame by means of an overhead slipring assembly. The thermistor bead has a low impedance so as to eliminate any concern with shielding from the water. The lead wires are protected in a one-foot long Omega Engineering alumina ceramic insulator tubing.

b. Results and Discussion

Before experiments with the thermistor were made in the cone geometry it was first tried in a rotating right circular cylinder, and it worked well. Due to certain indeterminate aspects of the thermistor operation in an oscillating flow, it is not intended that this section produce: absolute values of velocity inside the cone. So as not to appreciably disturb the interior flow, the voltage across the thermistor is turned on only after the interior flow has reached a steady state condition. In an oscillating flow of this type a continual amount of dissipated heat is put into essentially the same volume of water as it moves past the probe; this effect and that of the probe size on the velocity shear past it are areas of uncertainty. Hence the exact relation of δT to the axial vertical velocity measured by the probe is unknown.

Figures 8, 9, and 10 present the data obtained from the thermistor probe at the three axial heights above the apex of 5.13, 10.59, 15.5 cm. respectively. Each graph is a plot of peak to peak thermistor voltage, Δe , as recorded by the Varian, versus the turntable period given in seconds. The vertical solid lines on each graph are obtained from the theoretical curves of figure 5, and represent those values of turntable period T , at which a peak response is expected (only the first three are indicated on each graph). The thermistor results are in good
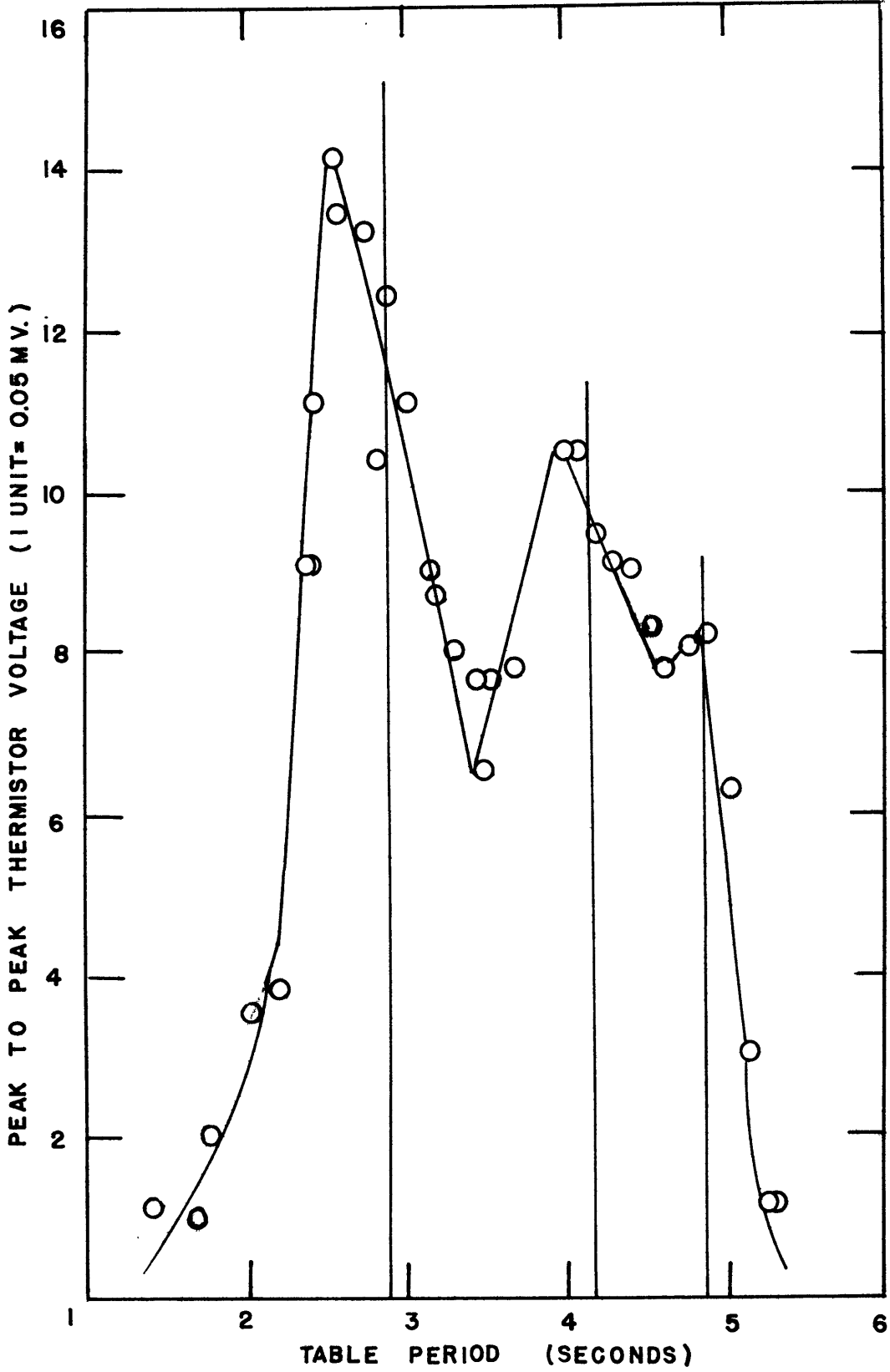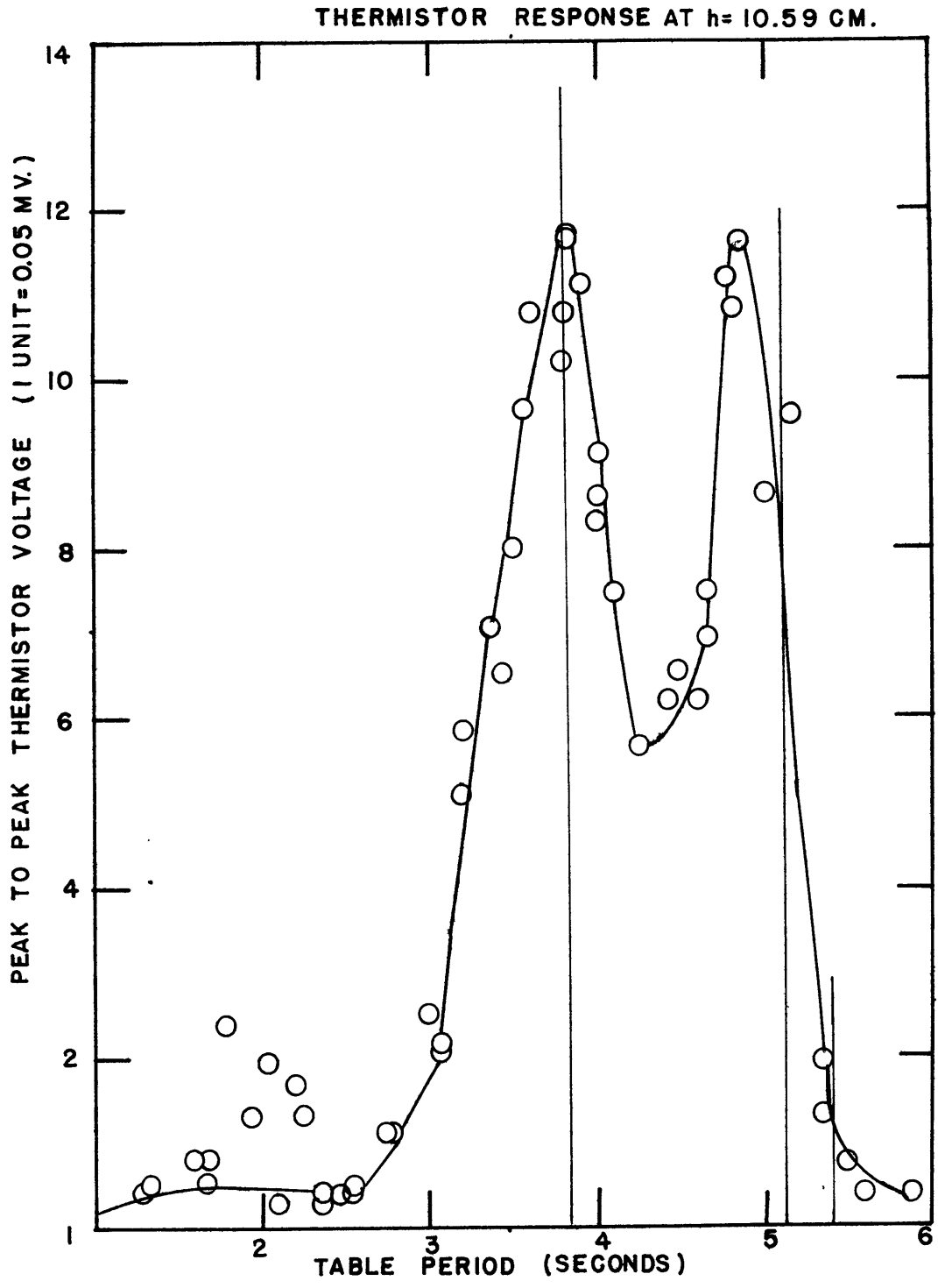
THERMISTOR RESPONSE AT h=5.13 CM.

FIGURE 8

FIGURE 9
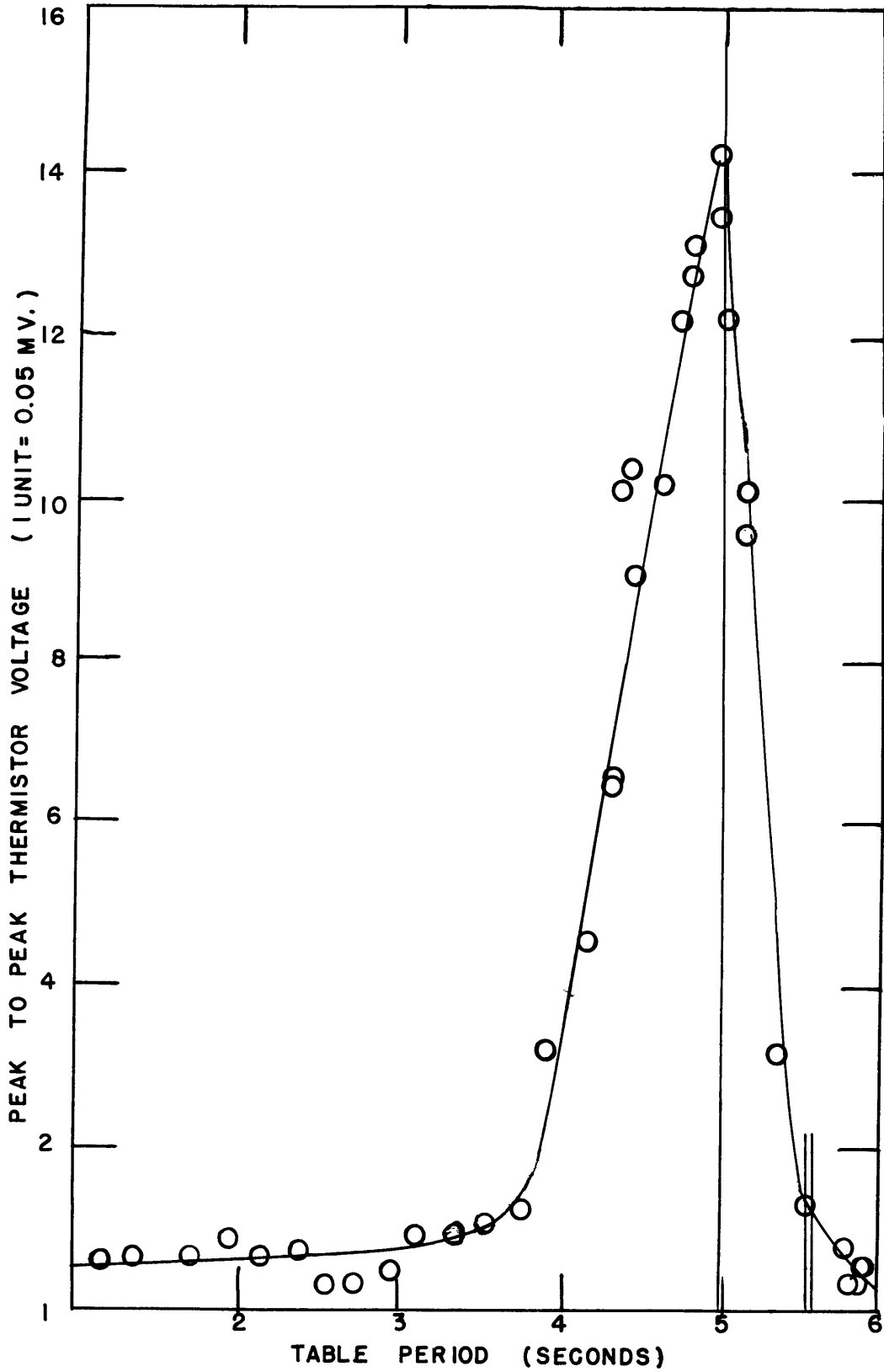
THERMISTOR   RESPONSE   AT   h= 15.5 CM.

FIGURE 10

agreement with these calculations except at the large turntable periods between 5 and 6 seconds. It is felt that this effect is due to the fluid velocities past the probe being near the minimum sensitivity threshold of the thermistor, since energy in the inertial wave is lost upon repeated reflections from the cone side walls.

3. Pressure Study

a. Introduction

The purpose of this section is to obtain an absolute determination of the pressure signals within the rotating right. circular cone as an aid in determining the properties of the interior motion. To accomplish this a pressure probe is positioned along the axis of the cone, with the general features of its response curve expected to be similar to figure 9 of the thermistor study. As a special study, the inside geometry of the cone was altered by placing a plug in the apex of the cone such that it now simulated a frustrum of a right cone of height 15.04 cm. The response curve from this particular geometry should have peaks similar to those from the cone study (figures 9 and 16) with extra peaks interspersed due to return reflection of energy as a consequence of the new bottom geometry. These extra peaks are felt to be resonance points in the frustrum.

b. Apparatus and Experimental Procedure

Because there is no return reflection of energy flux from the vertex, one does not expect resonance points in the cone but one does expect peak response at places where the direction of wave energy crosses the measuring position of the

pressure probe. Even in these cases of peak response, the signal level in the cone is quite small, in fact it is found that the signal to noise ratio is poor over the entire range of rotation speeds. Hence a type of power spectrum analysis had to be performed on the pressure output signal. Figure 11 is a schematic of the data gathering and data reduction equipment. A description of the Sanborn Pressure Transducer #268B and mating transducer converter #592-300 can be found in Aldridge (1967). I will briefly mention that the differentially operating transducer is connected to the fluid system with 1/4 inch tygon tubing, the complete system being free of bubbles (Kodak Photo Flow Solution helps) in order to obtain maximum response from the transducer. The interior of the transducer was adapted electrically to fit the system and is presented in figure 12. The pressure probe, a 10 inch long hyperdermic needle of .047 inch I.D., is mounted along the vertical axis of the cone at a height of 10,59cm. above the cone vertex, figure 13. The probe does not rotate with the cone but is independently suspended by means of a complex tripod arrangement critically weighted to minimize the random noise pickup of the transducer. Noise reduction played an important role in the design of the data gathering equipment. A filter (figure 14) of cutoff frequency 4 cps is incorporated after the converter to eliminate any 60 cycle pickup. Following the filter is a series of two amplifiers with a combined amplification factor of
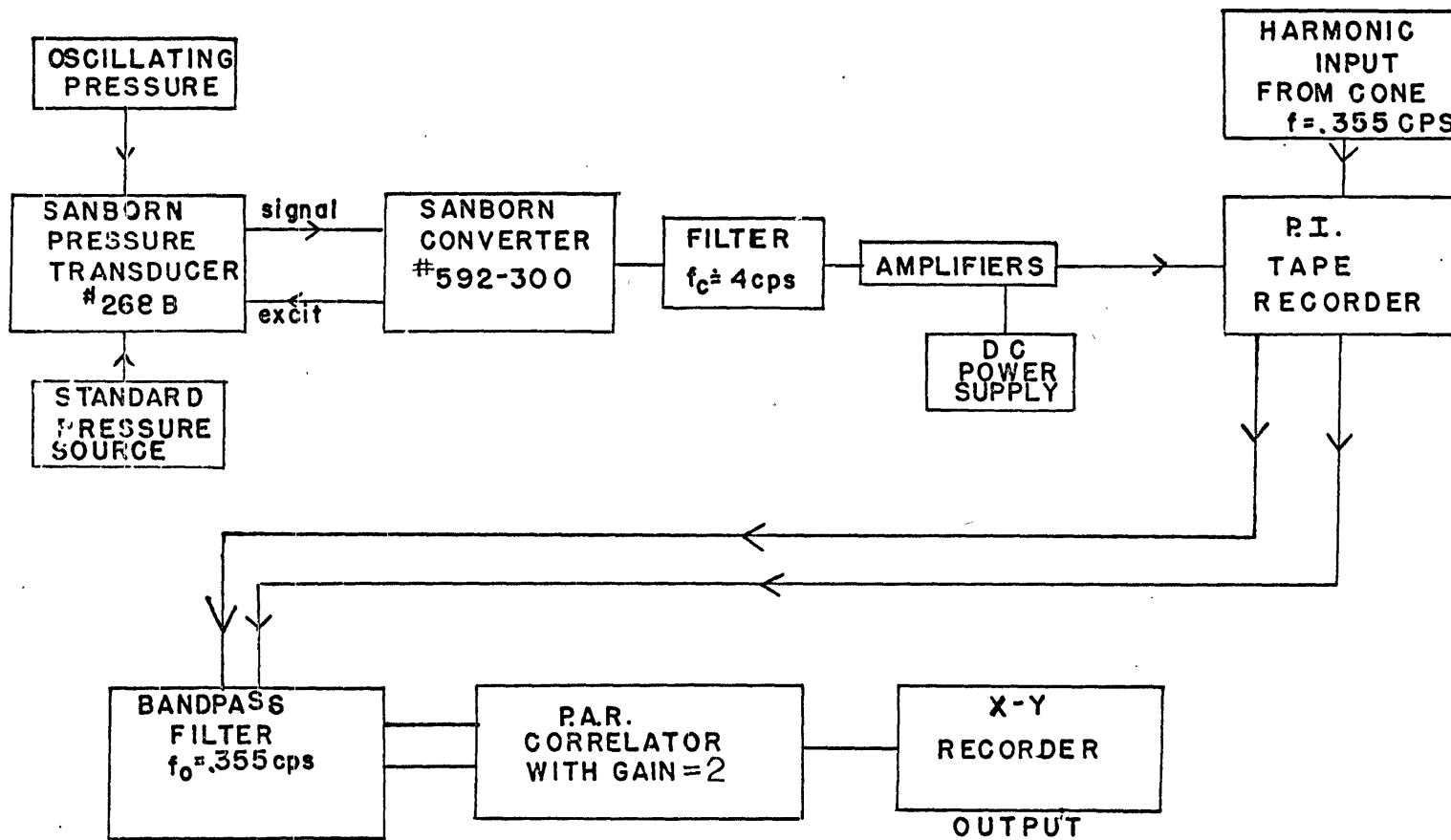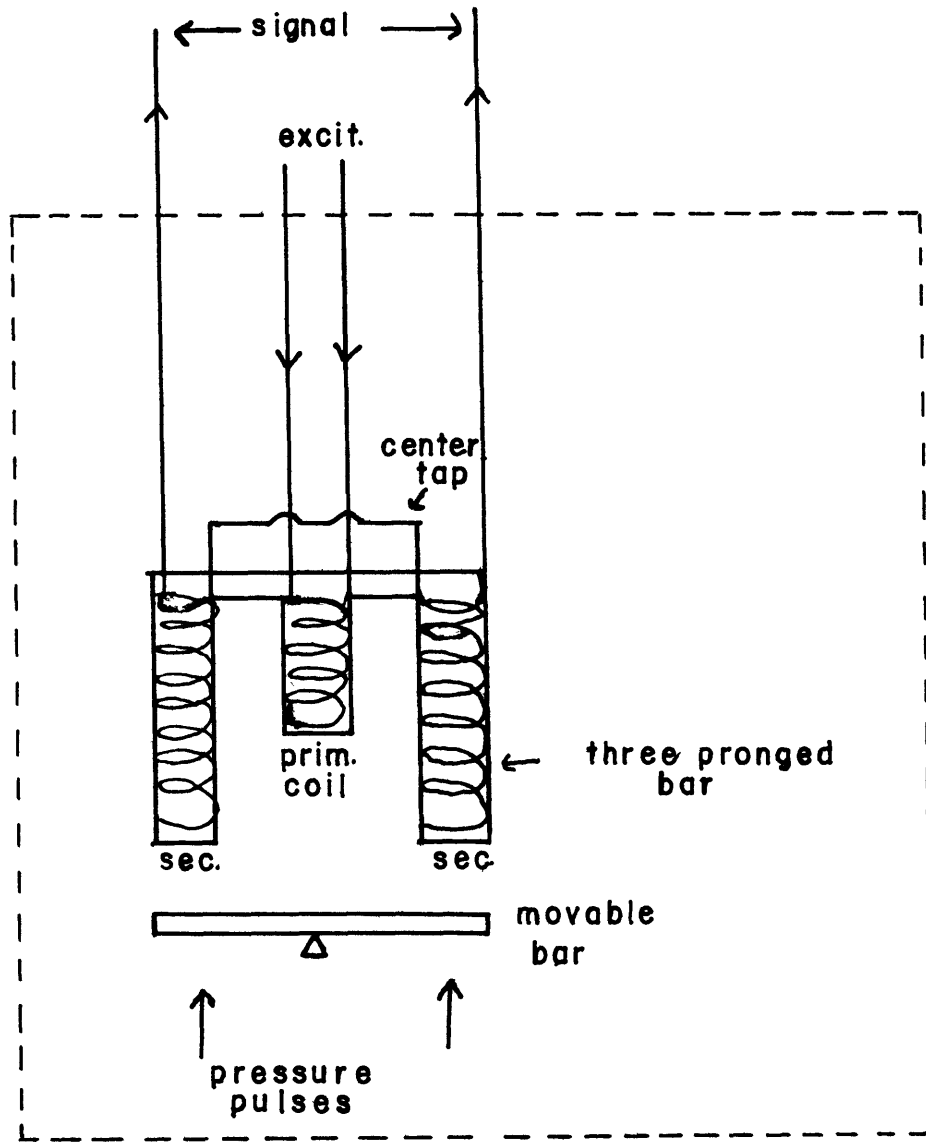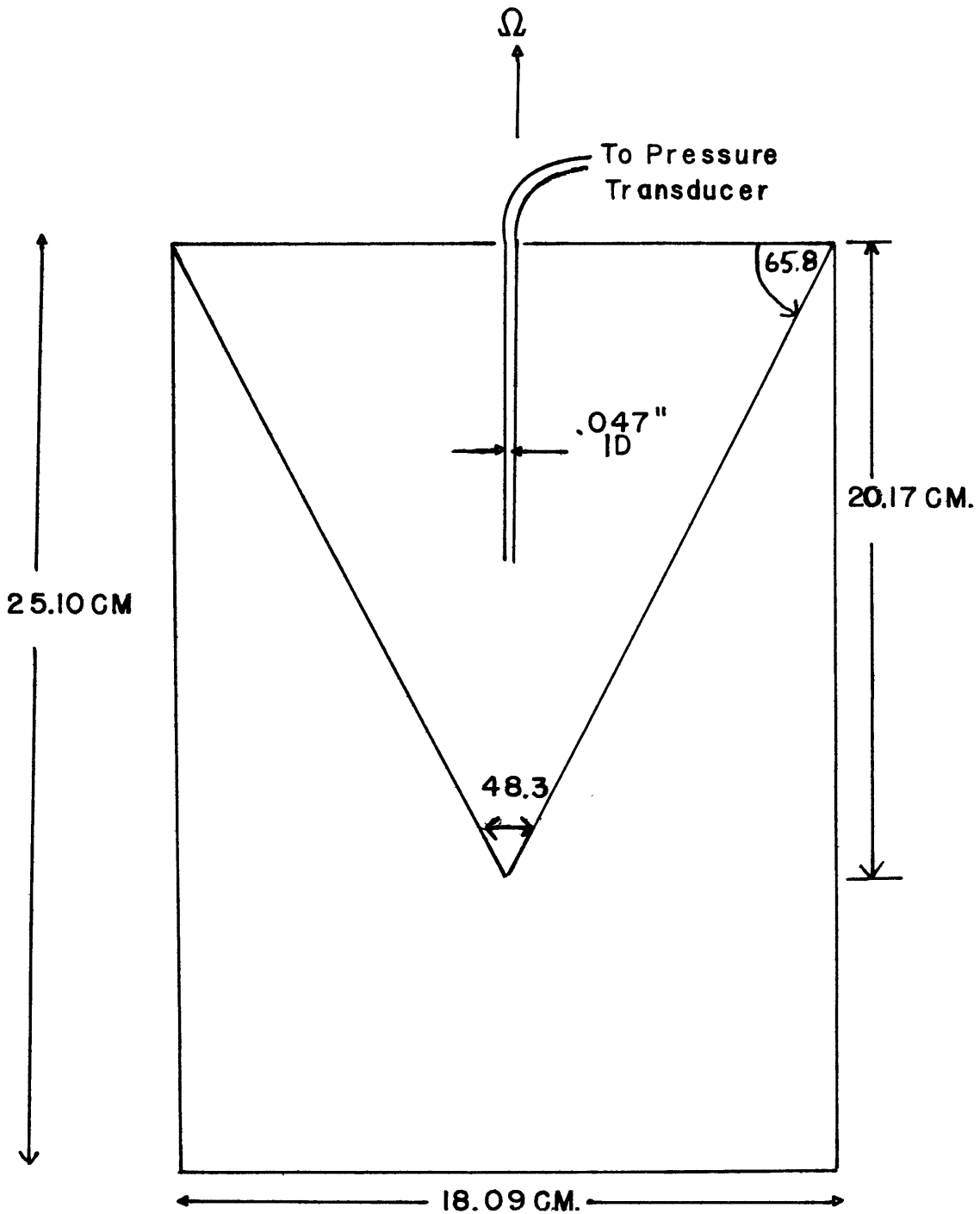
FIGURE II   SCHEMATIC OF DATA GATHERING AND REDUCTION EQUIPMENT

signal

excit.

center
tap

prim.
coil

three pronged
bar

sec.

sec.

movable
bar

pressure
pulses

TRANSDUCER
FIGURE 12

CONE
FIGURE 13

$\cong 10^5$. The first amplifier is a standard DANA model 2000 amplifier of total amplification factor $\cong 10^3$. In series with this is a bias controlled operational amplifier with a saturation level of ± 13 Volts. Ultimately the data is gathered on magnetic tape with a Precision Instrument four channel tape recorder, model 6200.

The data reduction equipment consists of further filtering of the taped pressure signal through an operational band pass filter with center frequency equal to the critical frequency of the cone oscillation, namely 0.355 cps. From this band pass filter the data is analyzed in a Princeton Applied Research correlator which essentially cross-correlates the pressure signals with a sinusoid which is recorded during the experimental runs on another channel of the tape recorder and is derived from a potentiometer circuit which directly measures the oscillation frequency of the cone, figure 15. The correlator determines the phase and amplitude of the pressure signal which then is recorded directly onto an X - Y recorder.

if we let $f_c = a \sin \omega t$ be our signal representing the cone oscillation

and $f_s = b \sin(\omega t - \phi) + m(t)$ represent the pressure signal and noise

the correlation process consists of

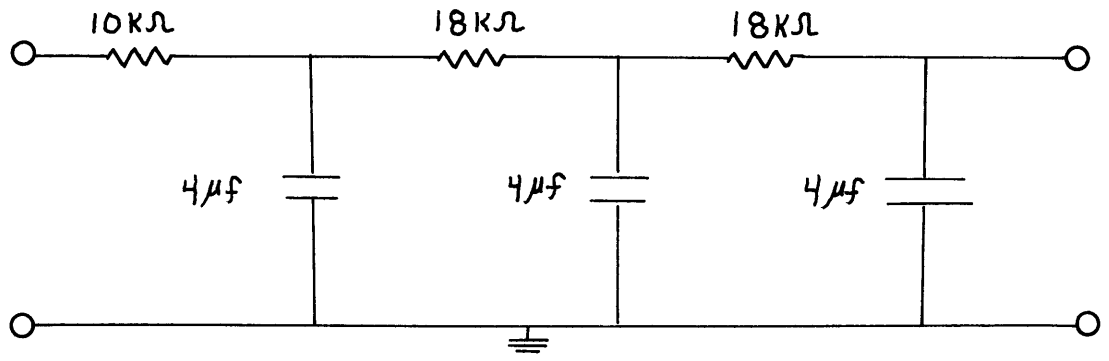$$C_{cs}(\tau) = \lim_{T \to \infty} \frac{1}{2T} \int_{-T}^{+T} f_c(t) f_s(t - \tau) \, dt$$

10KΩ   18KΩ   18KΩ

4μf   4μf   4μf

FIGURE 14

2490Ω

5.8V

1KΩ
TRIM POT.

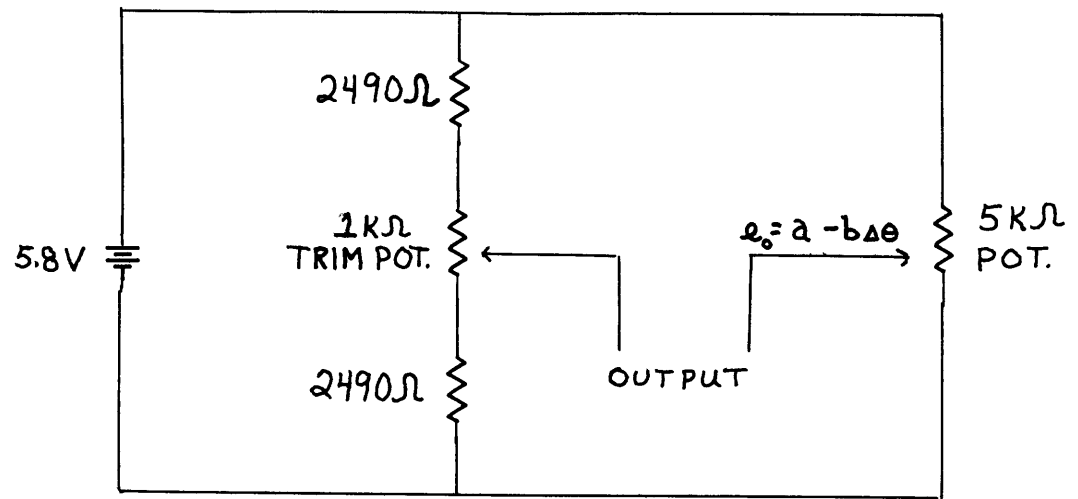$e_o = a - b\Delta\theta$

5KΩ
POT.

2490Ω

OUTPUT

FIGURE 15

-24-

which in our case yields $C_{cs}(t) = \frac{a\,b}{2} \cos(\omega t + \phi)$

ϕ being the phase shift.

The output is printed on the X - Y recorder as a cosine wave shifted along the T axis ϕ radians (representing the phase) and of amplitude equal to the magnitude of the pressure signal.

With the frustrum geometry, the support equipment used is identical with that employed in the cone study. The plug in the bottom of the cone has a diameter of 4.6 cm,, and the height of the frustrum is 15.04 cm. The pressure probe was again placed at 10.59 cm. above the vertex of the cone which is 5.46 cm. above the base of the frustrum.

c. Results and Discussion

In order to obtain absolute pressure readings inside the cone it was first necessary to calibrate the pressure transducer using a calibration stand which would simulate the oscillating pressure in the cone. Also a phase calibration was performed on the experimental apparatus to determine the phase lag or lead, if any, between the oscillating pressure signal and the cone position. A discussion of the pressure and phase calibrations appears in appendix A, the results of which have been used to obtain the absolute pressure curves of this section.

The results of the pressure study are presented in figures

16 and 17. These figures are plots of $\frac{\Delta P_A}{\rho g}$, the peak to
peak pressure displacement in $mm\ H_2O$, versus turntable
period in seconds. The three vertical dotted lines on each
graph represent the turntable periods at which peak response
is expected along the axis of the cone for the prescribed
probe heights. The curves are in excellent agreement with
these calculations determined from figure 5. As mentioned
earlier in the text, it was expected that the two response
curves would have similar shapes and would have equivalent
pressure magnitudes. The extra peak at T = 3.3 seconds for
the frustrum is a resonance peak due to back reflection of
energy, it is the only one which stands out on this response
curve but does give a clear indication that resonances can be
induced in the cone by altering the vertex geometry. One should
also notice the fine agreement with the thermistor response
curve, figure 9, for $\Theta < 65° \Rightarrow T_T > 2.4$ seconds (characteristics
lying within the cone). The anomalous large pressure response
at table periods of $\sim 2^S$ cannot be explained at present but
is thought to be a result of disruption of the interior flow
since the characteristics from the upper corner are predicted
to lie outside the cone. The flow separation in these cases
must react with the boundary layers along the side walls to
cause large pressures along the axis.

AXIAL PRESSURE RESPONSE IN CONE

TURNTABLE   PERIOD   (SECONDS)
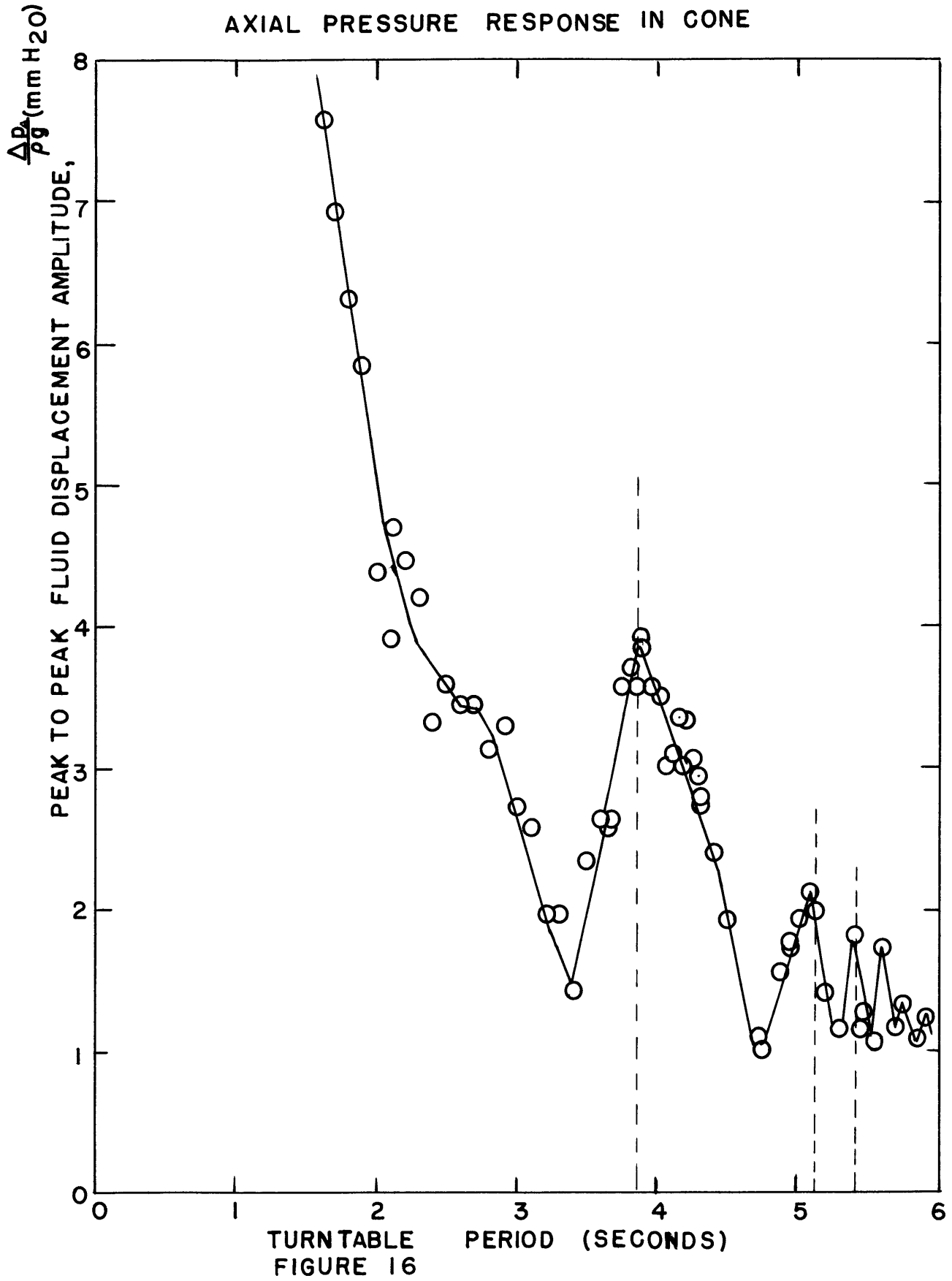
FIGURE 16

AXIAL PRESSURE RESPONSE IN FRUSTRUM
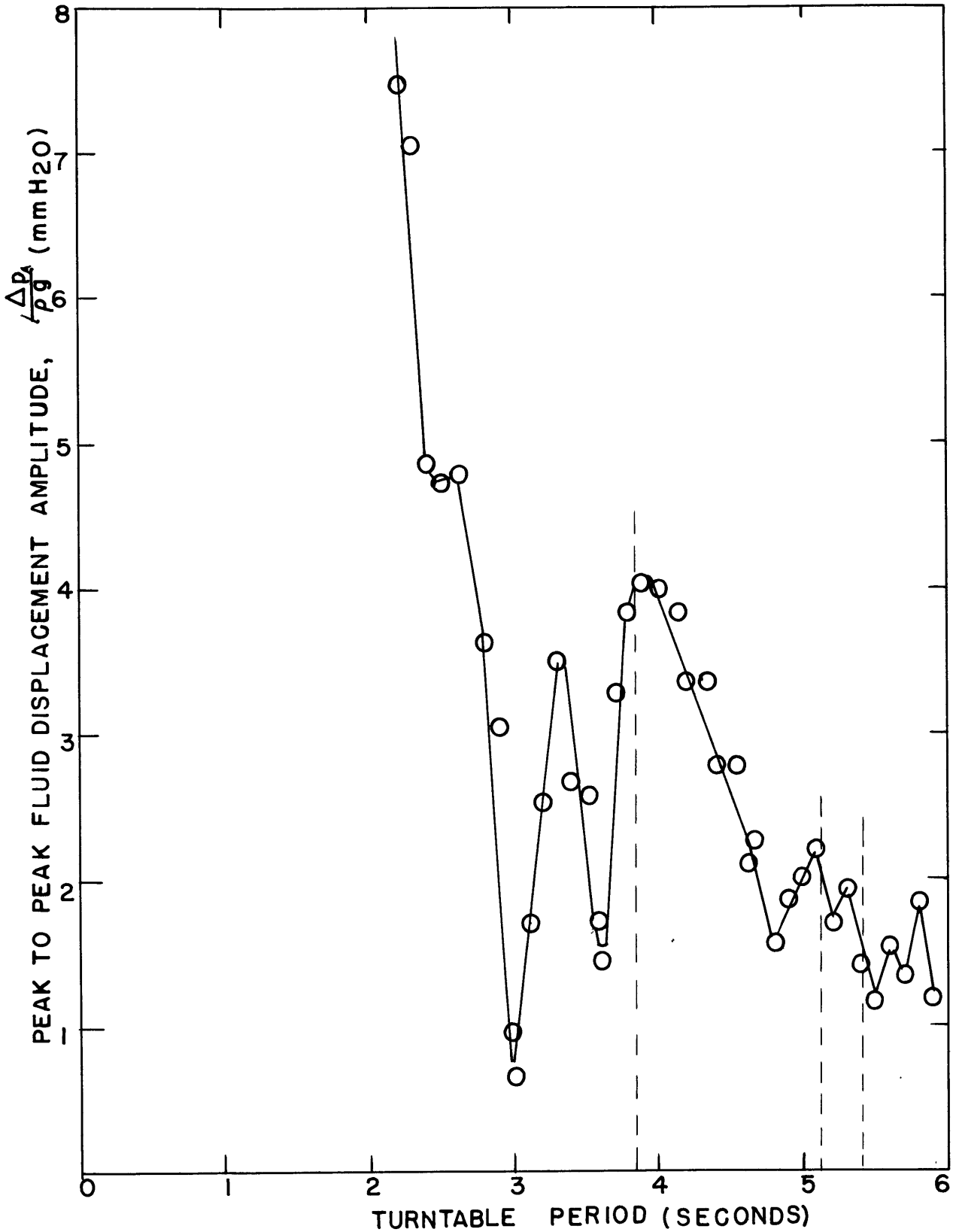

FIGURE 17

4. Visual Study

a. Apparatus and Experimental Procedure

Two interesting types of photographs of the cone's interior flow can be utilized for data analysis and reduction. The first type is a view of a vertical cross-section of the cone illustrating the characteristics (usually of a darker shade than the rest of the flow) emanating from the upper corners of the rotating body and subsequently reflecting off the sloping side walls on their trip toward the "infinite-well" apex at the bottom of the cone. Utilizing the fact that the interior flow is symmetric, as will be shown in the photographs at the end of this section, the choice of positioning one's camera and light source either both inside or outside the rotating frame is left to the photographer's discretion. This first type of photograph can be found in Greenspan (1969). The second type of photograph, those which I took, are intended to bring out more detail especially of the particle motion in the flow field. These photographs capture the horizontal flow structure, since the camera is mounted parallel to a plane perpendicular to the rotation axis. The light source (G. E. 100 watt projection lamp) is similarly mounted in the rotating frame and produces a thin (0.3 cm. and o.6 cm. in the two experimental cases) horizontal beam, parallel to the plane of the camera, which intersects the cone at the height of 10.59 cm.

-30-

above its apex. This particular height was chosen as it was
also the axial positioning of the thermistor and pressure
probes, affording a three-way comparison of the numerical and
visual data.

The cone is filled with a suspension of distilled water
and large aluminum flakes, wet with a common detergent to
prevent unnecessary clinging to the side walls. The aluminum
flakes were washed beforehand with acetone which broke up any
large globules which had formed.

A Nikon-F 35 mm. camera is used with a special automatic
film winder to advance the film while the table rotates. (The
film used is Kodak Tri-X Pan fast black and white which worked
best with all exterior lighting eliminated).

Refer to figure 18 for a schematic of the support equip-
ment for visual studies. In order to correlate the timing of
the pictures with the cone oscillation period an electric circuit
was designed using a potentiometer which directly measures the
oscillation of the cone. The output of the circuit is connected
via power sliprings to a Beckman dynagraph recorder. See
figure 19 and 20 for the circuit design and its output. The
sinusoid in the output refers to the motion of the harmonically
oscillating cone, and the spikes correspond to the times of
camera activation and turn off respectively. The camera acti-
vation,and exposure length is controlled by a Cramer type 540
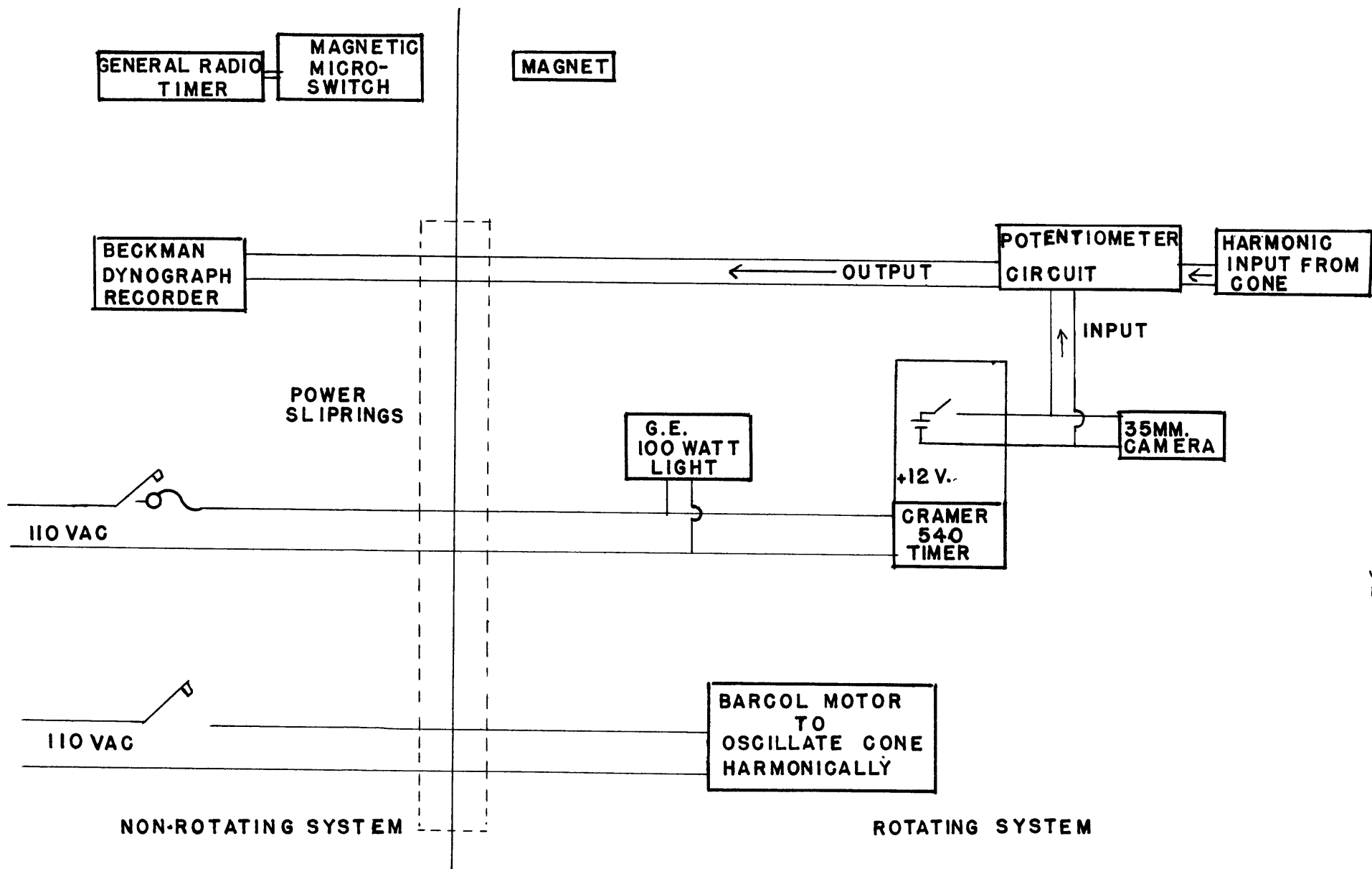timer, and the turntable rotation speed (accurate to $< 0.2\%$)

GENERAL RADIO TIMER

MAGNETIC MICRO-SWITCH

MAGNET

BECKMAN DYNOGRAPH RECORDER

POTENTIOMETER CIRCUIT

HARMONIC INPUT FROM CONE

← OUTPUT

↑ INPUT

POWER SLIPRINGS

G.E. 100 WATT LIGHT

35MM. CAMERA

+12 V.

110 VAC

CRAMER 540 TIMER

110 VAC

BARCOL MOTOR TO OSCILLATE CONE HARMONICALLY

NON-ROTATING SYSTEM

ROTATING SYSTEM

FIGURE 18   SCHEMATIC OF SUPPORT EQUIPMENT FOR VISUAL STUDIES

is measured with a magnetic reed switch circuit coupled to a
General Radio timer. If we represent the motion of the cone
with a cosine curve as illustrated in figure 21, and divide
the oscillation period into eighths of a period then $t = 0$,
$T/2$, T represent times of maximum amplitude of the oscillation
just as the action of a spring-weight system undergoing simple
harmonic motion with $t = 0$ representing the spring in the
stretched position.

b. Explanation of Two Features of the Photographs

This section is intended to be a short discussion on two
features of the photographs which the author feels are not in-
herently obvious.

1) Radius of particle orbit versus particle velocity

A balance of the forces acting on the particle in its cir-
cular orbit inside the cone are, (figure 22).

$$\left| f_{coR} \right| = \left| f_{cent} \right|$$

$$m \, 2\Omega r = m \nu^2 / r$$

recalling that $\qquad \nu = \Omega \, r$

we obtain $\qquad r = \dfrac{\nu}{2} \qquad or \qquad r \propto \nu$

This relation tells us that the radius of the path is
directly proportional to the particle velocity. With this rel-
ation a glance at the photographs will reveal that the particle
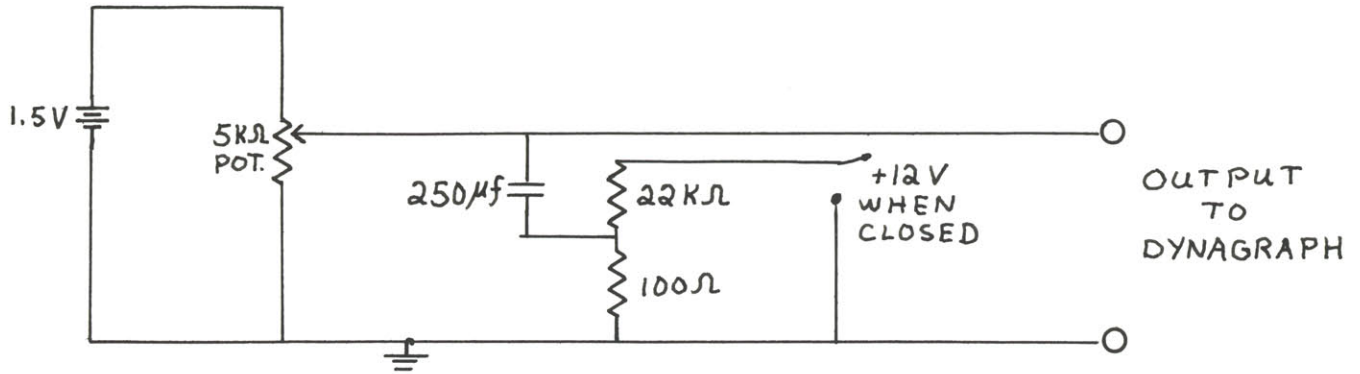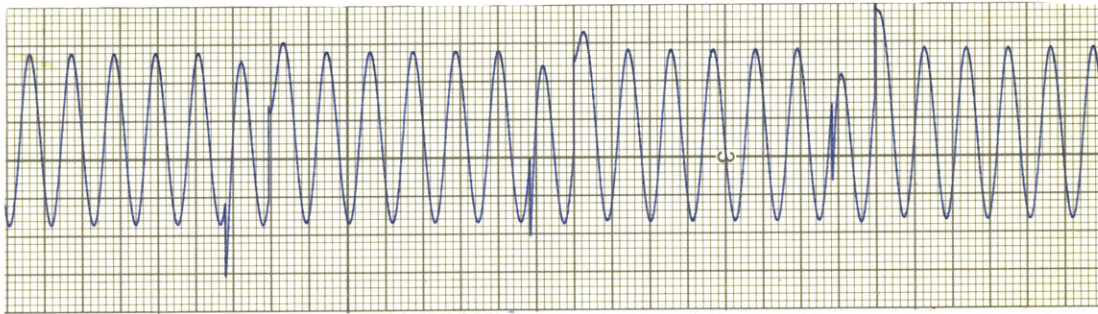speed is greatest near the characteristics with velocity decreas-
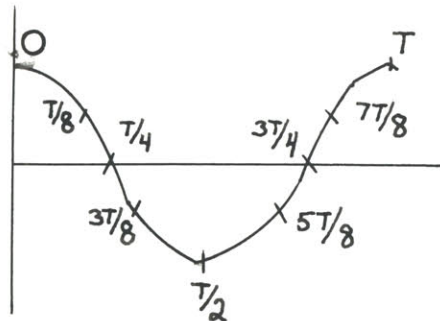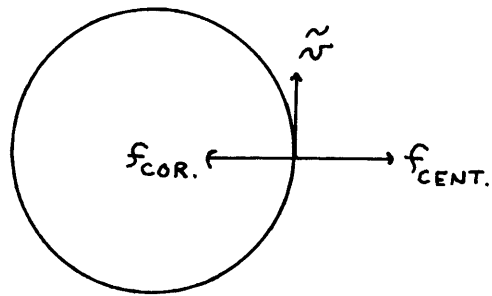
FIGURE 19

FIGURE 20

FIGURE 21

FIGURE 22

ing in toward the center and outward toward the wall. A review

of figure 9 illustrates that a turntable period of $T_T = 3.85$ seconds

lies in a region of peak thermistor response whereas that of

$T_T = 3.00$ seconds lies in a valley on the response curve. Thus

a relation such as $r \propto \mathcal{N}$ was expected since the pictures at a

turntable period of $T_T = 3.85$ seconds indicate larger circular

orbits in general, than do the ones at a turntable period of

$T_T = 3.00$ seconds.

2) Apparent ellipticity of the motion and a determination
   of the direction of energy propagation

The particle motion has been postulated to be circular,

why then does it appear to be elliptical in the pictures? The

answer is that the particle motion which is along the characteris-

tics is not in the same plane as the camera. This perspective

anomaly can be checked mathematically. If we let ℓ_1 represent

the major axis of the circular orbit and ℓ_2 represent the minor

axis, then from elementary trigonometry we find that

$$\ell_1' = \ell_1 \cos \theta = r \cos \theta$$

if motion is indeed circular where

$$\ell_2' = \ell_2 = r$$

$\ell_1' \, \zeta \, \ell_2'$ are the axes of the orbit

shown on the photographs

therefore the ratio of major to minor axis on the pictures should

be $\epsilon = \dfrac{\ell_1'}{\ell_2'} = \cos \theta$ Values for the respective parameters are pre-

sented in the following table.

T_T	θ	$\cos \theta$	EXPERIMENTAL VALUES
3.00	$57° 51'$	0.532	$0.56 \pm .03$
3.85	$46° 55'$	0.683	$0.67 \pm .03$

An analysis of the photographs show $\epsilon \propto \cos\theta$. Thus we can say that the particle motion is circular with the direction of energy propagation along the characteristics. It is instructive here to mention that ϵ is not exactly $= \cos\theta$ but merely proportional to it since there is a slight counter-clockwise drift around the cone superimposed on the circular particle motion.

c. Summary of Visual Study

Following is a discussion of the main features of the interior, horizontal structure as deduced solely from analysis of the streak photographs. All conclusions in this summary are elucidated further in the photographs of part d.

The basic turntable rotation is clockwise when looking down at the photographs. The pictures taken with the two different light beam thicknesses (0.3 and 0.6 cm.) are identical indicating that the actual amplitude of the particle motion (radius of the inertia circle) is small. Photographs were also taken at two different turntable periods $T_T = 3.85$ and $T_T = 3.00$ seconds. From the previous discussion, one would expect that the $T_T = 3.85$ second photos would have an overall larger amplitude of motion and this fact is indeed bourne out. Using equation B-5 of appendix B, one determines that the characteristics should cross near the center for the $T = 3.85$ second

pictures and at 0.6 R out from the center for the $T_T = 3.00$
second pictures. With this information, one determines from
the photographs that the amplitude of the particle motion is
greatest near the characteristics with decreasing amplitude
in toward the center or out toward the wall (edge of photo).
Analysis of the $T_T = 3.00$ second pictures reveals a smoothly
changing particle phase of about 90° through the characteristic
region, e.g. the phase of the particle motion is changing near
the characteristics such that the phase on either side of the
characteristic is different. Away from the influence of the
characteristics the phase appears constant. Sequences of
photographs were taken at times of 5, 15, and 20 minutes after
start of spin up. Those at the same part of the oscillation
period for the three different times are identical proving
that once spin up is reached the motion is time invariant.
Further reduction indicates that the interior motion can be
divided into three regimes:

1) An interior motion which is influenced by the position
of the characteristics, this is the largest region on the photos.

2) A central core of small but varying thickness. The
motion in this core appears minute possibly due to its vertical
nature.

3) A boundary layer of thickness $\sim R/5$ but again of vary-
ing size depending on the characteristic position. The cone

side walls radically affects the motion in the boundary layer near them. The magnitude of the particle motion in the boundary layer is the same for different rotation speeds. The particle motion in all the pictures is counterclockwise and circular. Superimposed on this counterclockwise circular motion is a counterclockwise drift around the cone. One would be more accurate in describing the motion as eddylike. Since the particle motion is counter-clockwise, the phase on the inside of the characteristics is found to lead that on the outside. Photographs taken for different exposure times of 0.9, 1.4 and 2.8 seconds display that the particles make one revolution every oscillation period (2.83 seconds).

To summarize one can say that the general features of the interior flow are similar for different rotation speeds providing the characteristics lie within the cone, with parameters such as phase, amplitude of motion, boundary layer thicknesses, and velocities being directly influenced by the position of the characteristics. All aspects of the flow are continuous.

d. Discussion of Photographs

In the photographs which follow the four parameters used to distinguish each one are:

T_T , turntable period $= 3.85$, 3.00 seconds

T_c , camera exposure time $= 0.9$, 1.4, 2.8 seconds

T_{osc} , time of oscillation $=$ 0, T/8, T/4, 3T/8, T/2, 5T/8, 3T/4, 7T/8

W , light beam thickness $=$ 0.3, 0.6 cm.

Figures 23-29 illustrate the counter-clockwise particle motion inside the cone. The phase changes smoothly by approximately 1/8 period for each successive picture. The black X marks the approximate center of each photograph, the lines being radii of approximately the same angular position on each photo. The large black dot is not the center but a vacuum seal on the top of the cone, with the bright rim being caused by the light beam as it passes through the cone side walls.

turntable period   = 3.85 seconds
camera exposure time = 1.4 seconds
time of oscillation   =   0
light beam thickness = 0.6 cm.
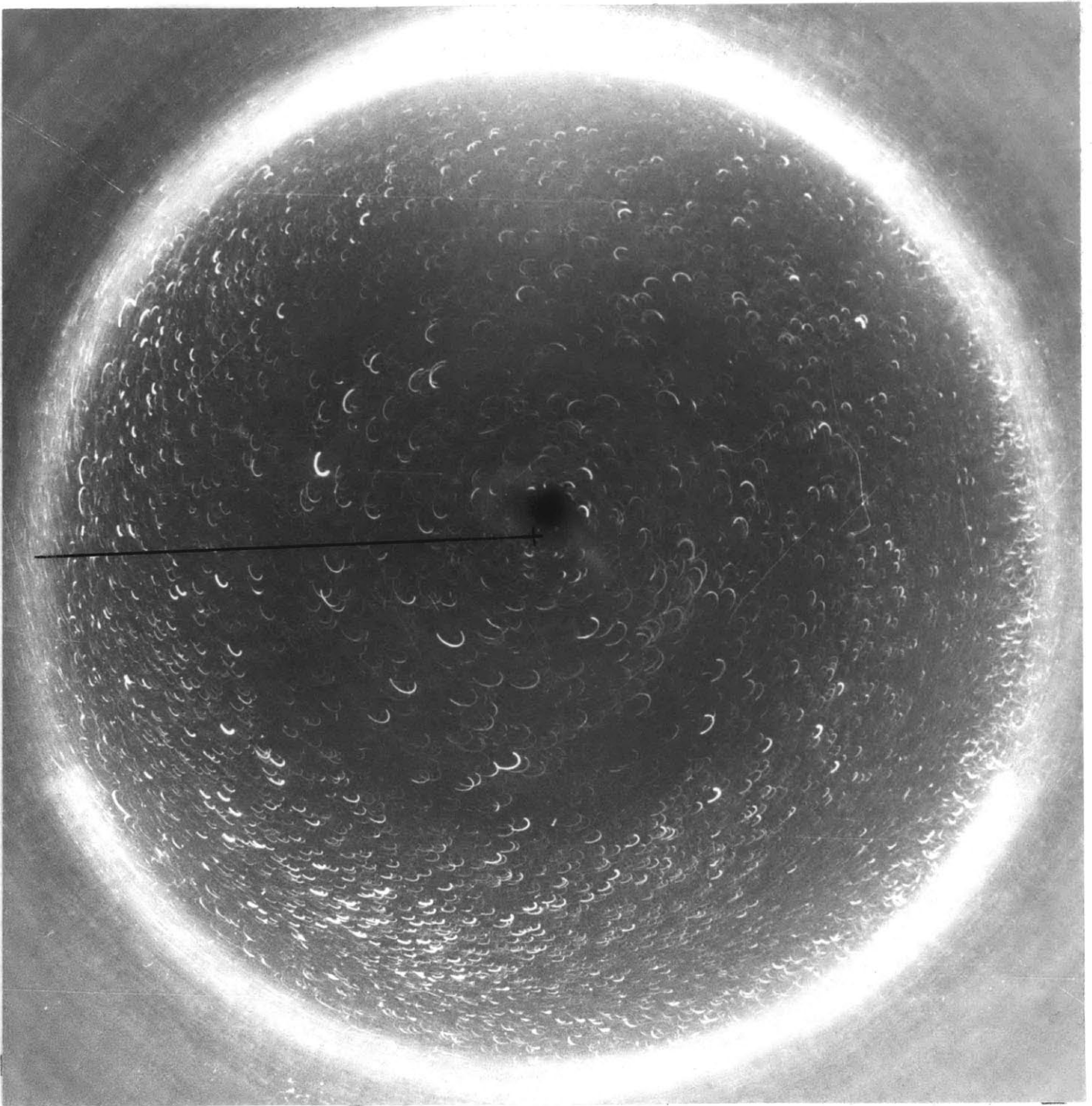
FIGURE 23

turntable period   = 3.85 seconds
camera exposure time = 1.4 seconds
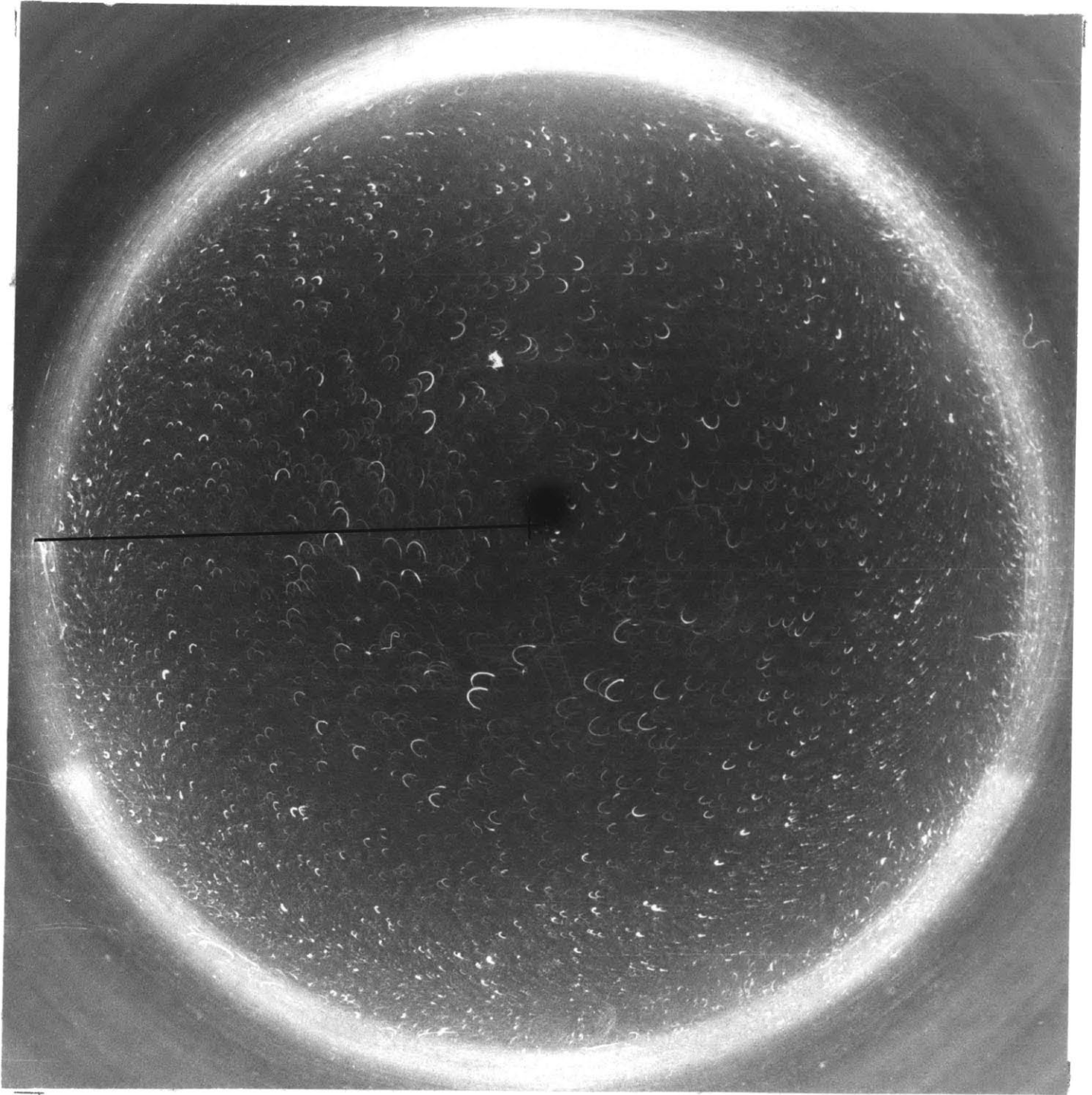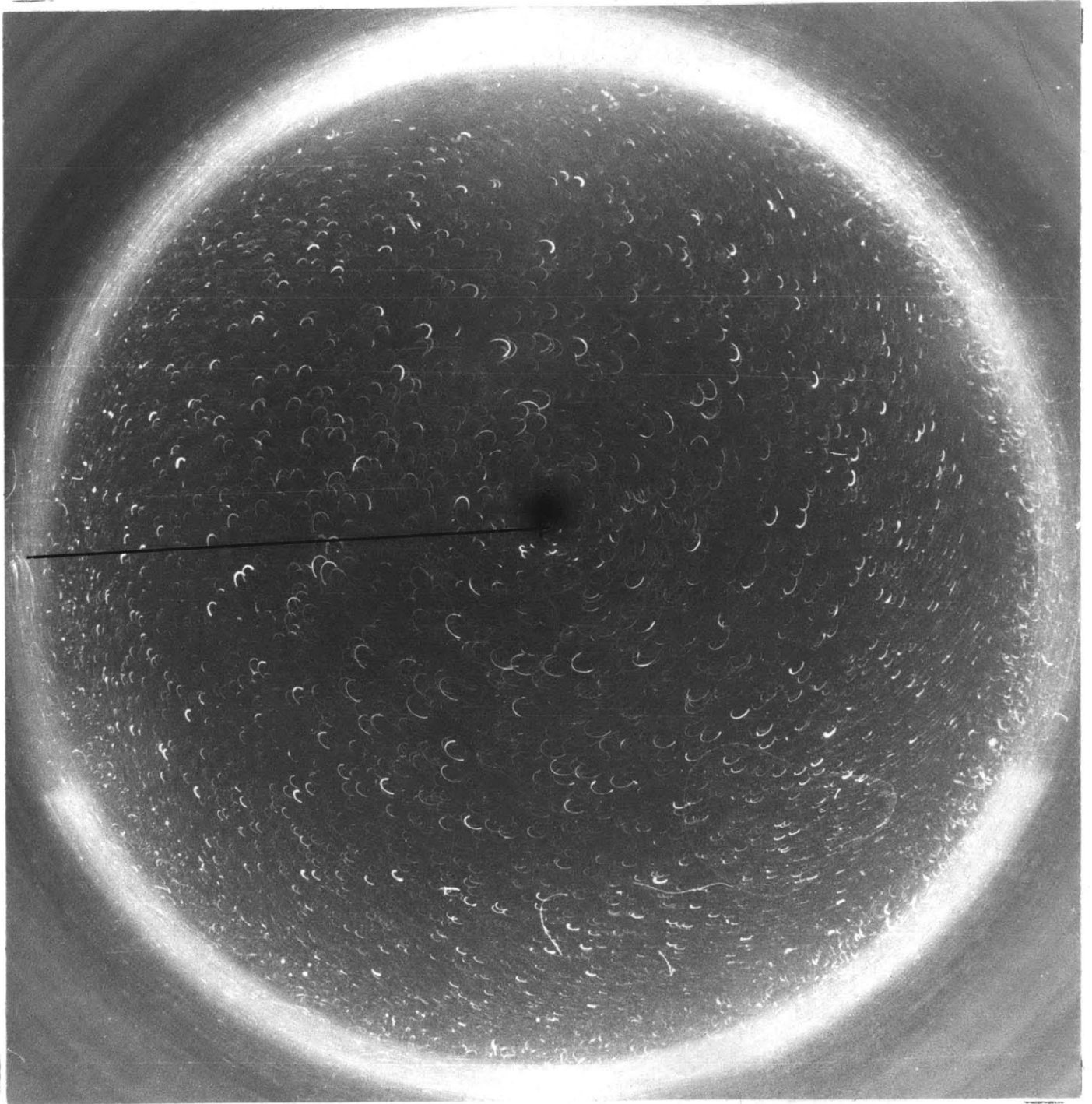time of oscillation = T/8
light beam thickness = 0.6 cm.
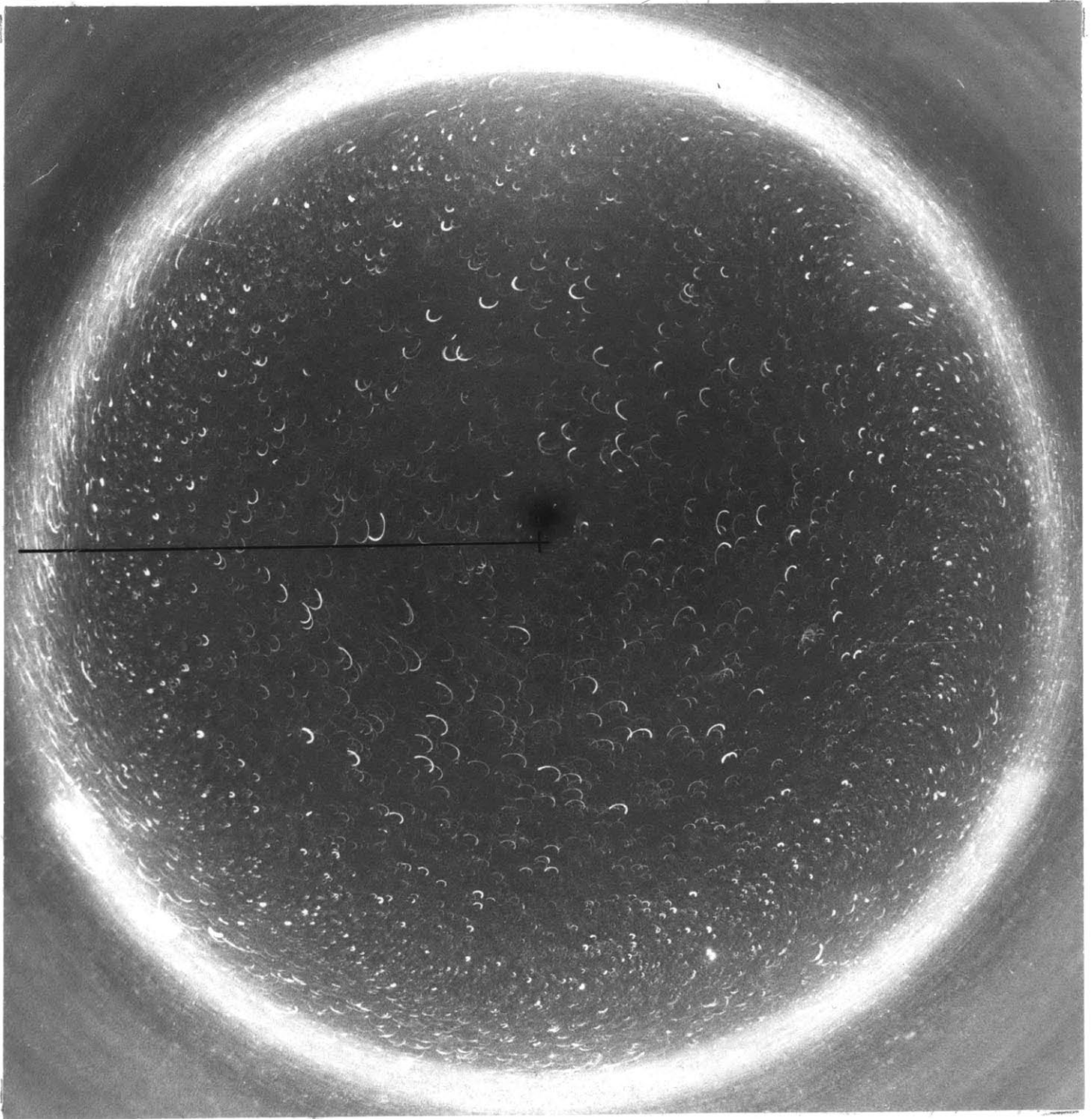
FIGURE 24

turntable period   = 3.85 seconds
camera exposure time = 1.4 seconds
time of oscillation = 3T/8
light beam thickness = 0.6 cm.
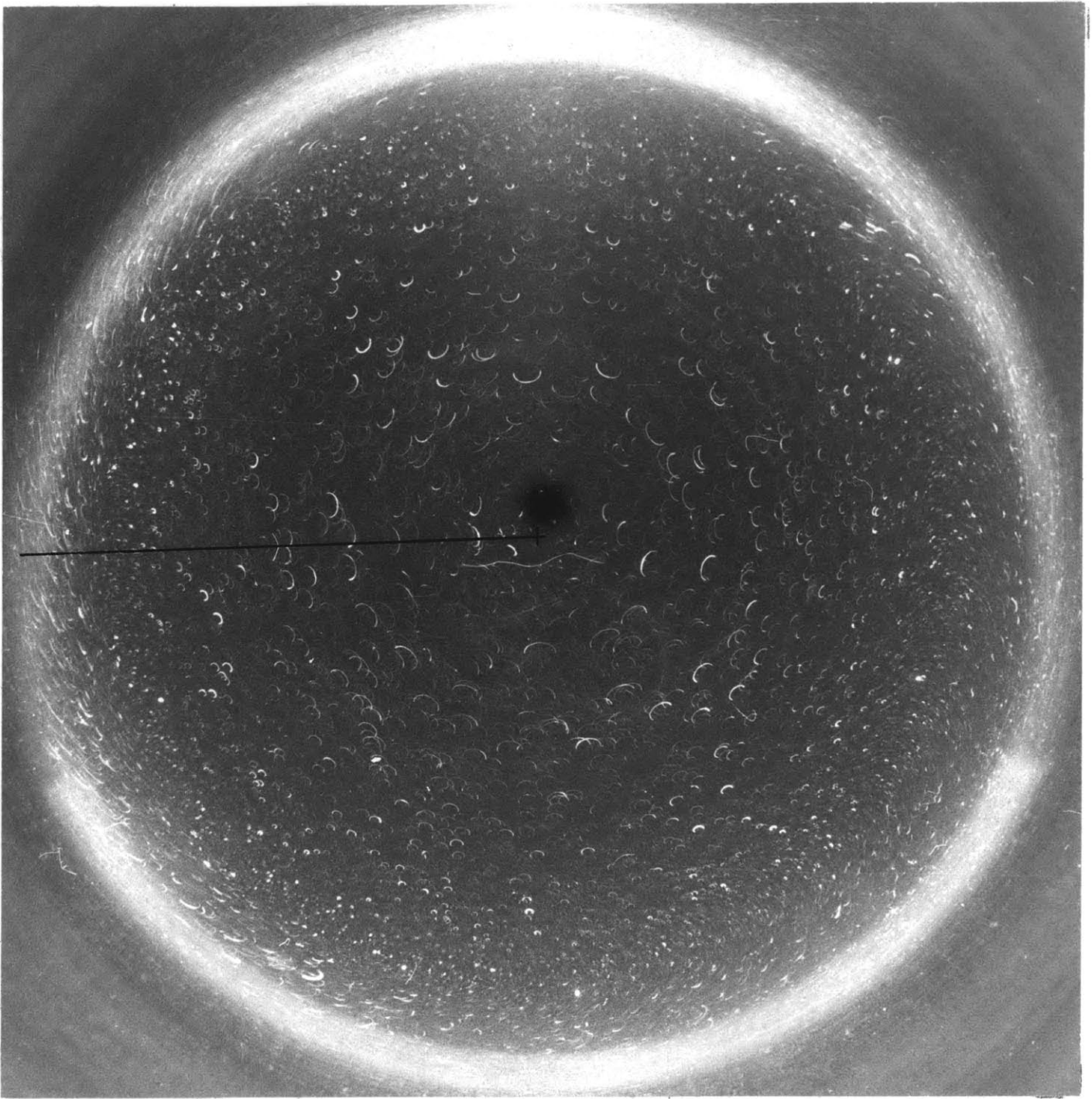
FIGURE 25

turntable period   = 3.85 seconds
camera exposure time = 1.4   seconds
time of oscillation = T/2
light beam thickness = 0.6   cm.
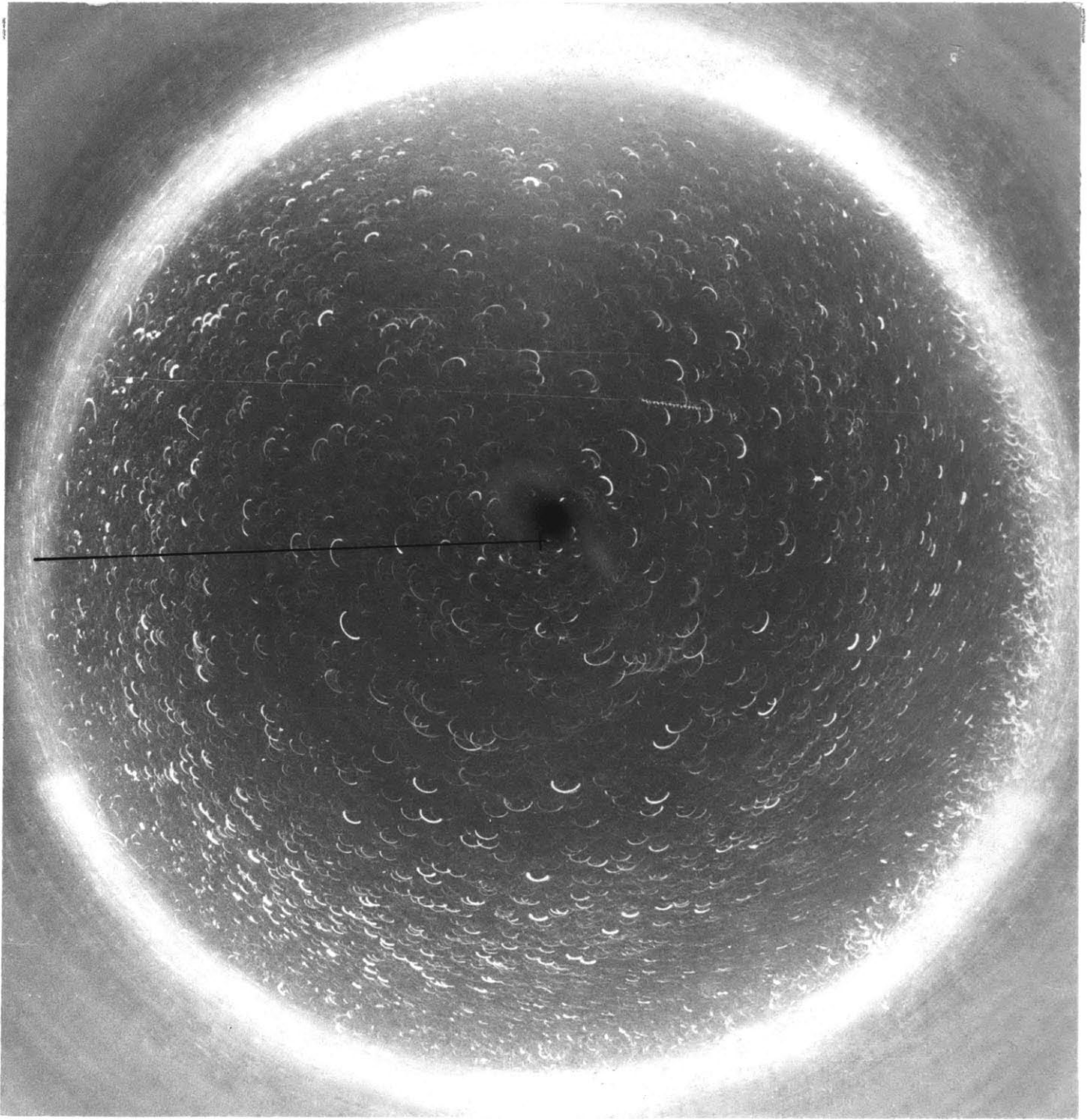

FIGURE 26

In figures 23-29, theory predicts that
the characteristics will cross at the center.
The amplitude of the particle motion is seen
to increase from the edge of the photo reach-
ing a maximum near the center. The phase re-
mains constant along any given radius.

turntable period   = 3.85 seconds
camera exposure time = 1.4 seconds
time of oscillation = 5T/8
light beam thickness = 0.6 cm.

FIGURE 27

turntable period   = 3.85 seconds
camera exposure time = 1.4 seconds
time of oscillation = 3T/4
light beam thickness = 0.6 cm.

FIGURE 28

turntable period   = 3.85 second
camera exposure time = 1.4   seconds
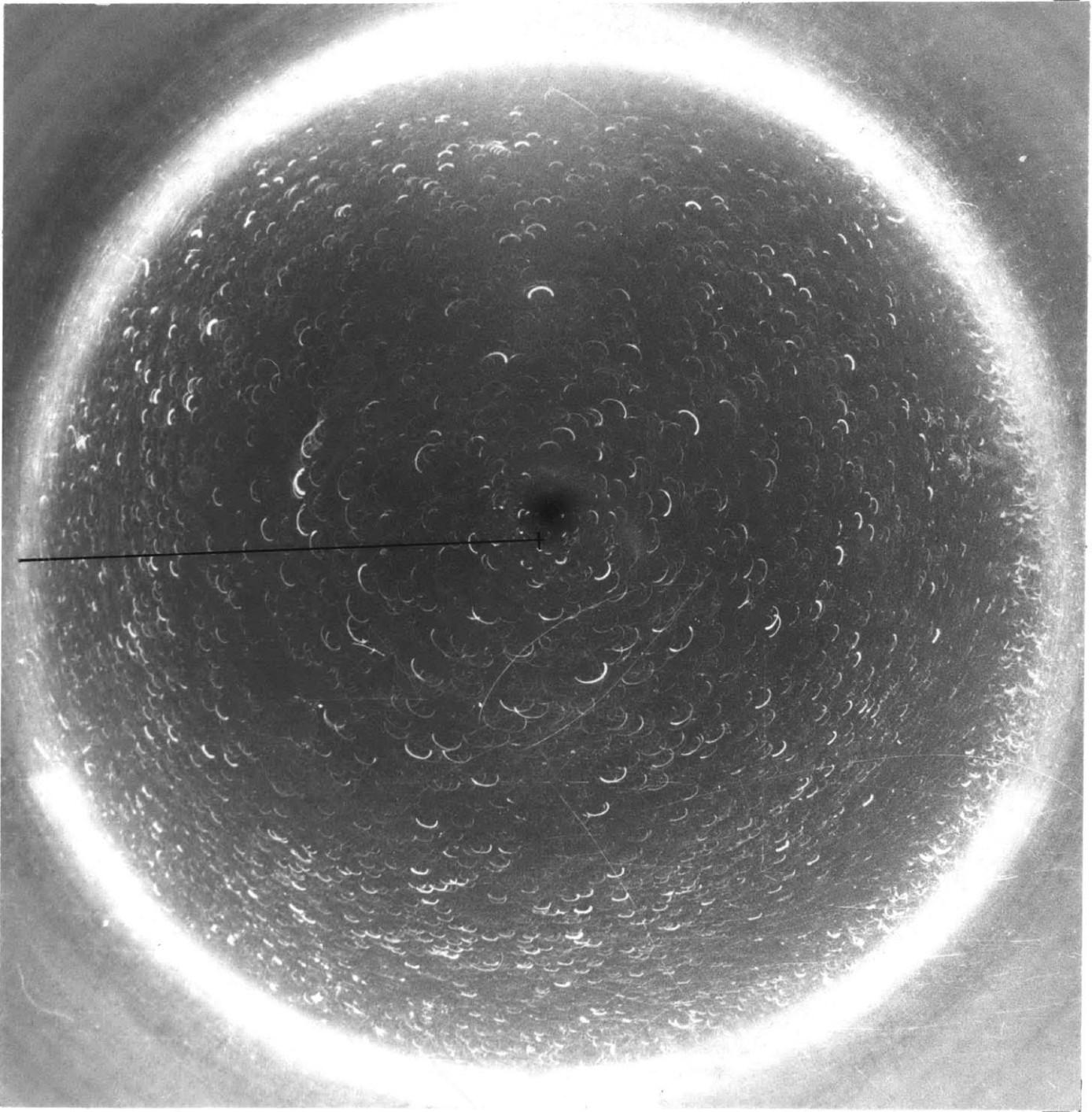time of oscillation = 7T/8
light beam thickness = 0.6   cm.

FIGURE 29

Figures 30, 31, 32, illustrate the time invariance of the interior flow. Figure 30 was photographed at 5 minutes after start of spin up, figure 31 at 15 minutes, and figure 32 at 20 minutes, and all three appear identical.

turntable period   = 3.85 seconds
camera exposure time = 1.4 seconds
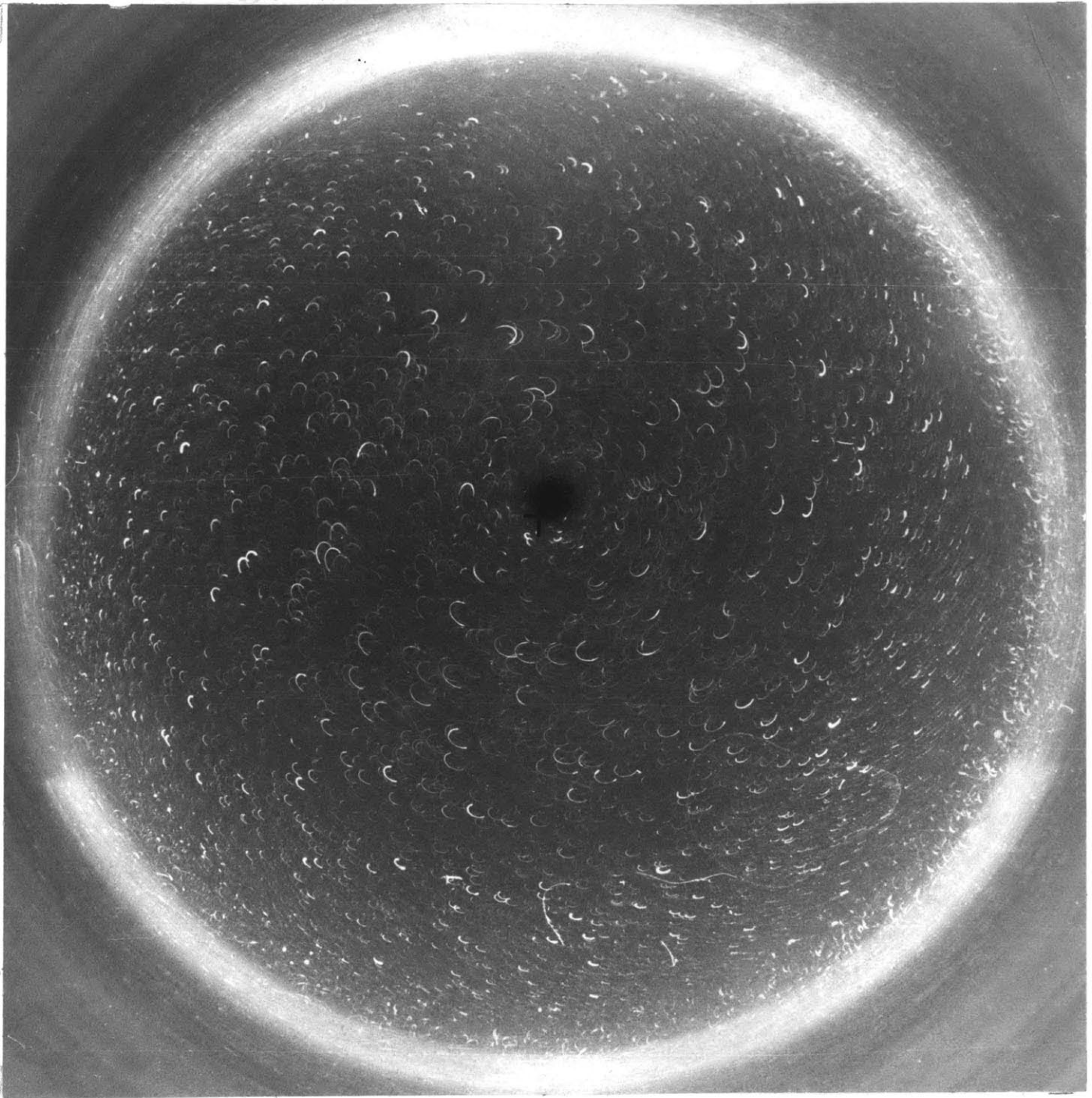time of oscillation = T/4
light beam thickness = 0.6 cm.

FIGURE 30

turntable period   = 3.85 seconds
camera exposure time = 1.4 seconds
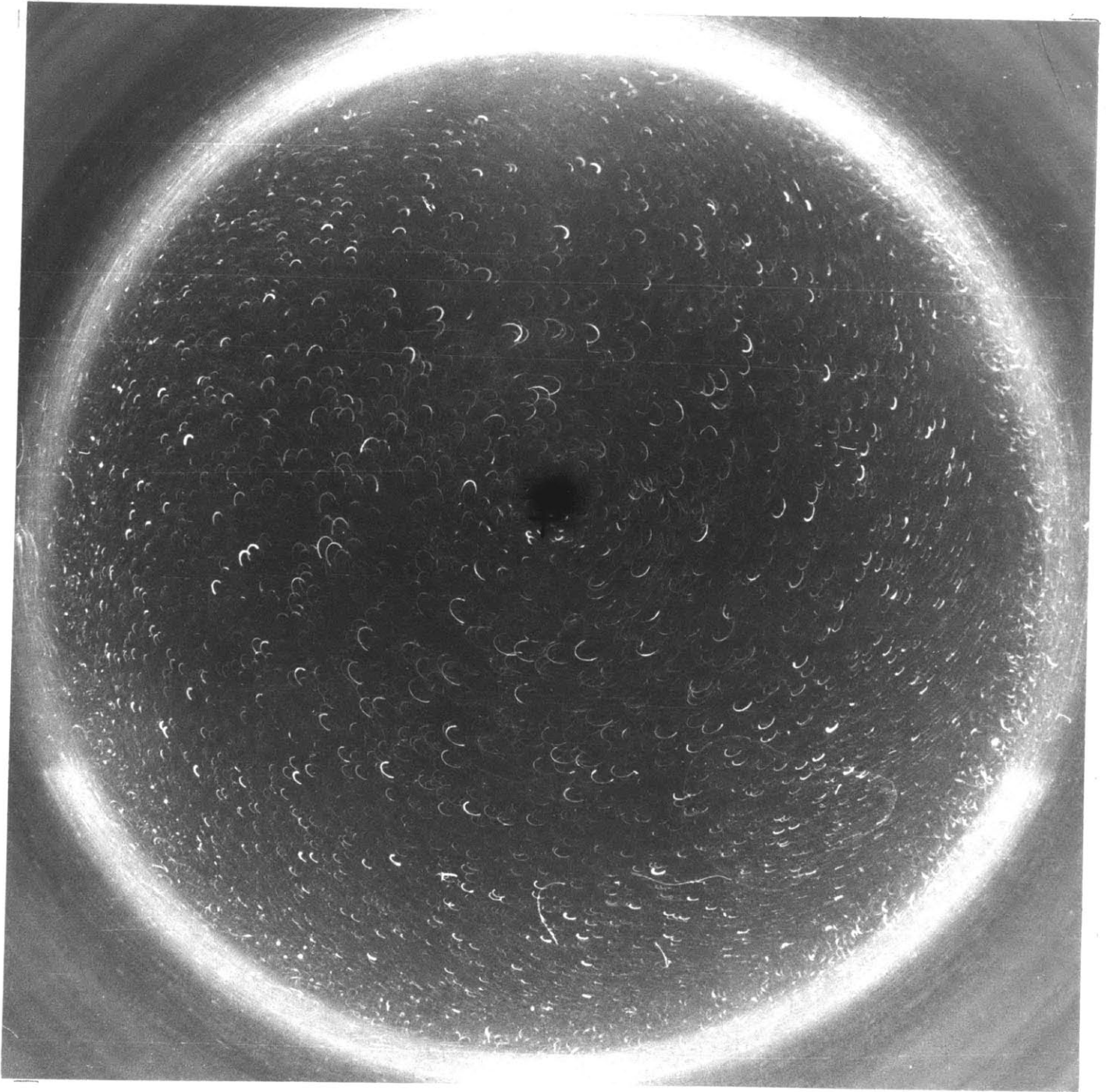time of oscillation = T/4
light beam thickness = 0.6 cm.

FIGURE 31

turntable period   = 3.85 seconds
camera exposure time = 1.4 seconds
time of oscillation = T/4
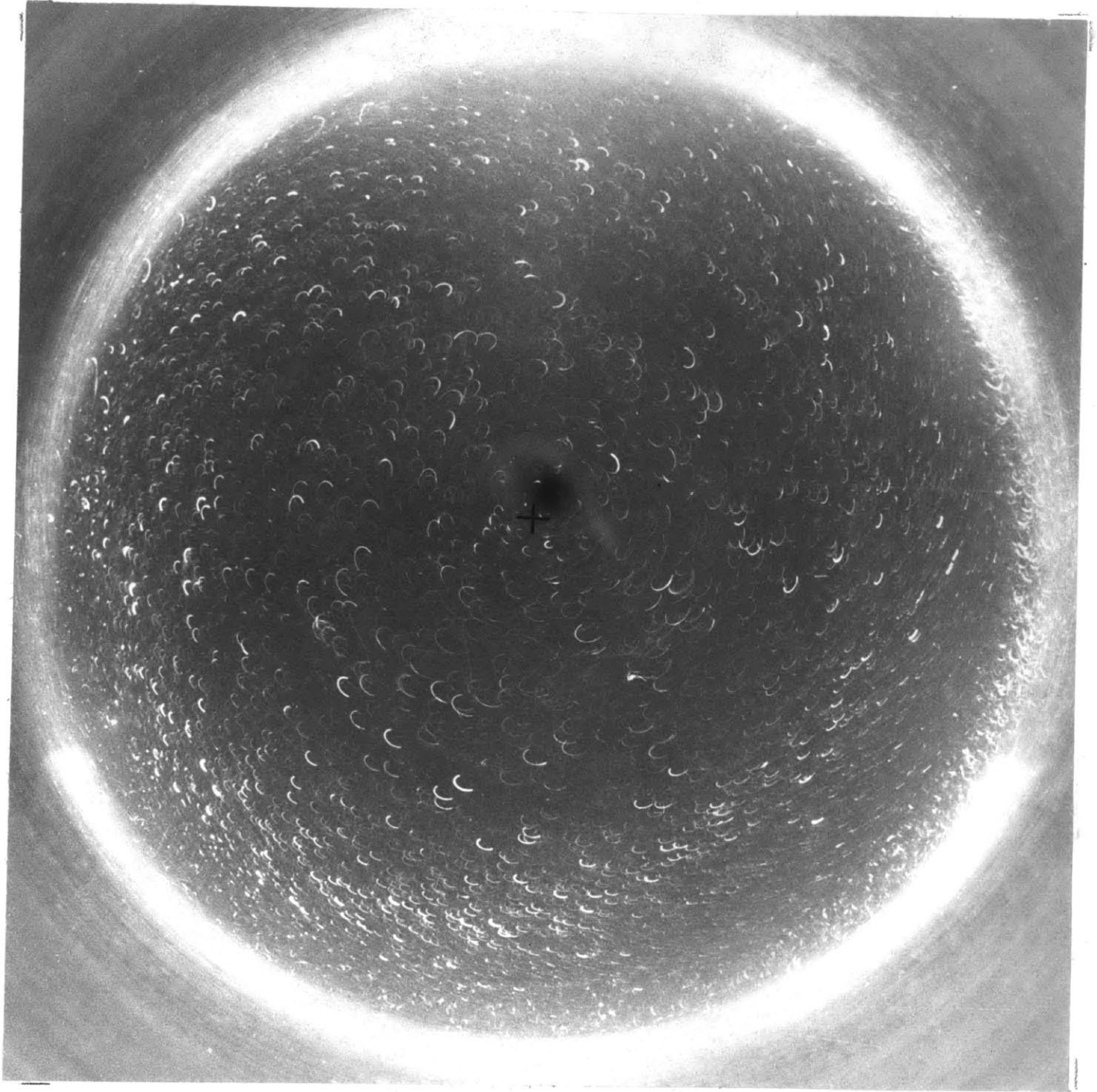light beam thickness = 0.6 cm.

FIGURE 32

Figures 33, 34, were photographed with different light beam thicknesses and are similar indicating that the particle motion is small.

turntable period   = 3.85 seconds
camera exposure time = 2.8 seconds
time of oscillation = T/4
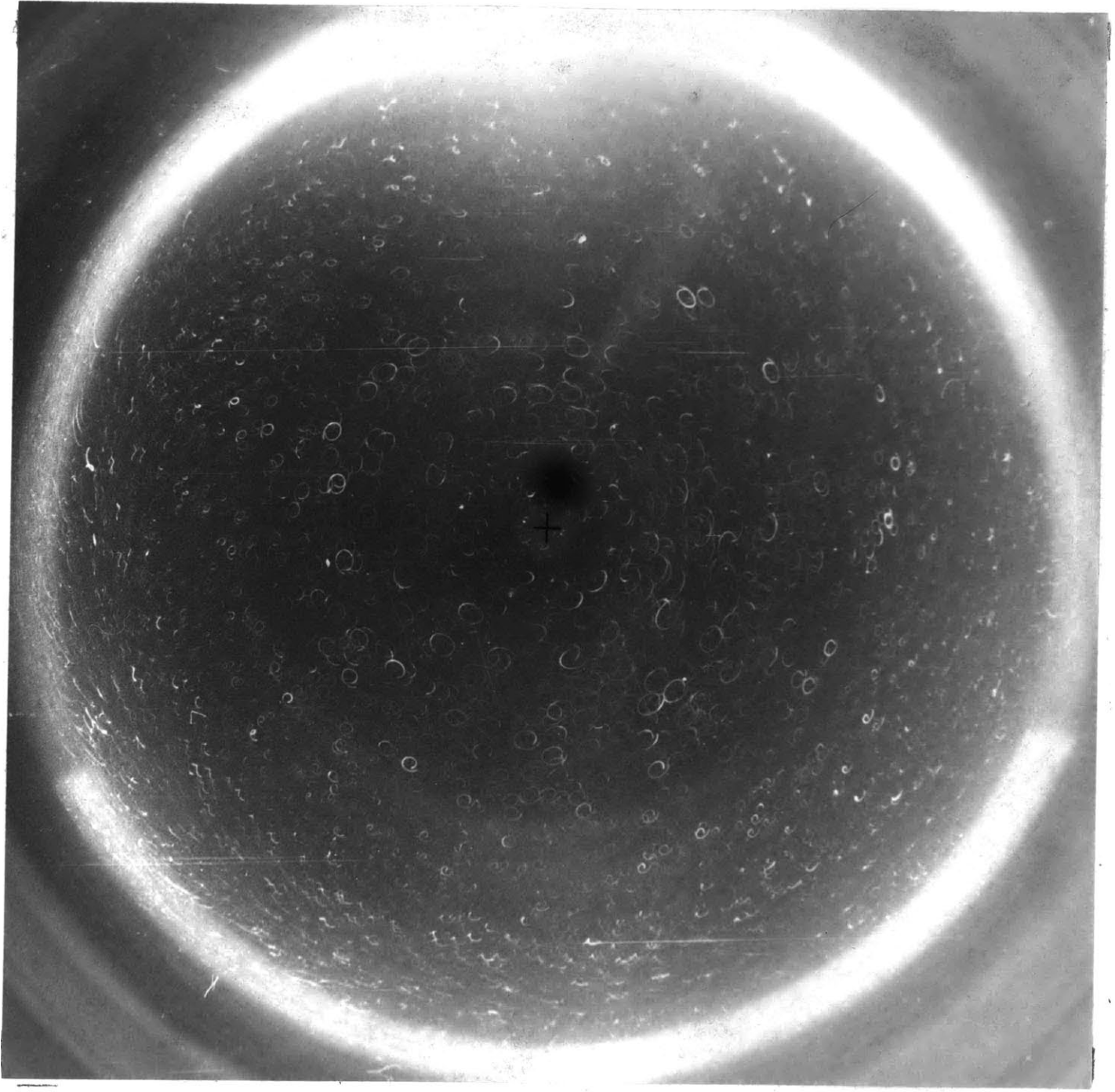light beam thickness = 0.6 cm.

FIGURE 33

turntable period   = 3.85 seconds
camera exposure time   = 2.8 seconds
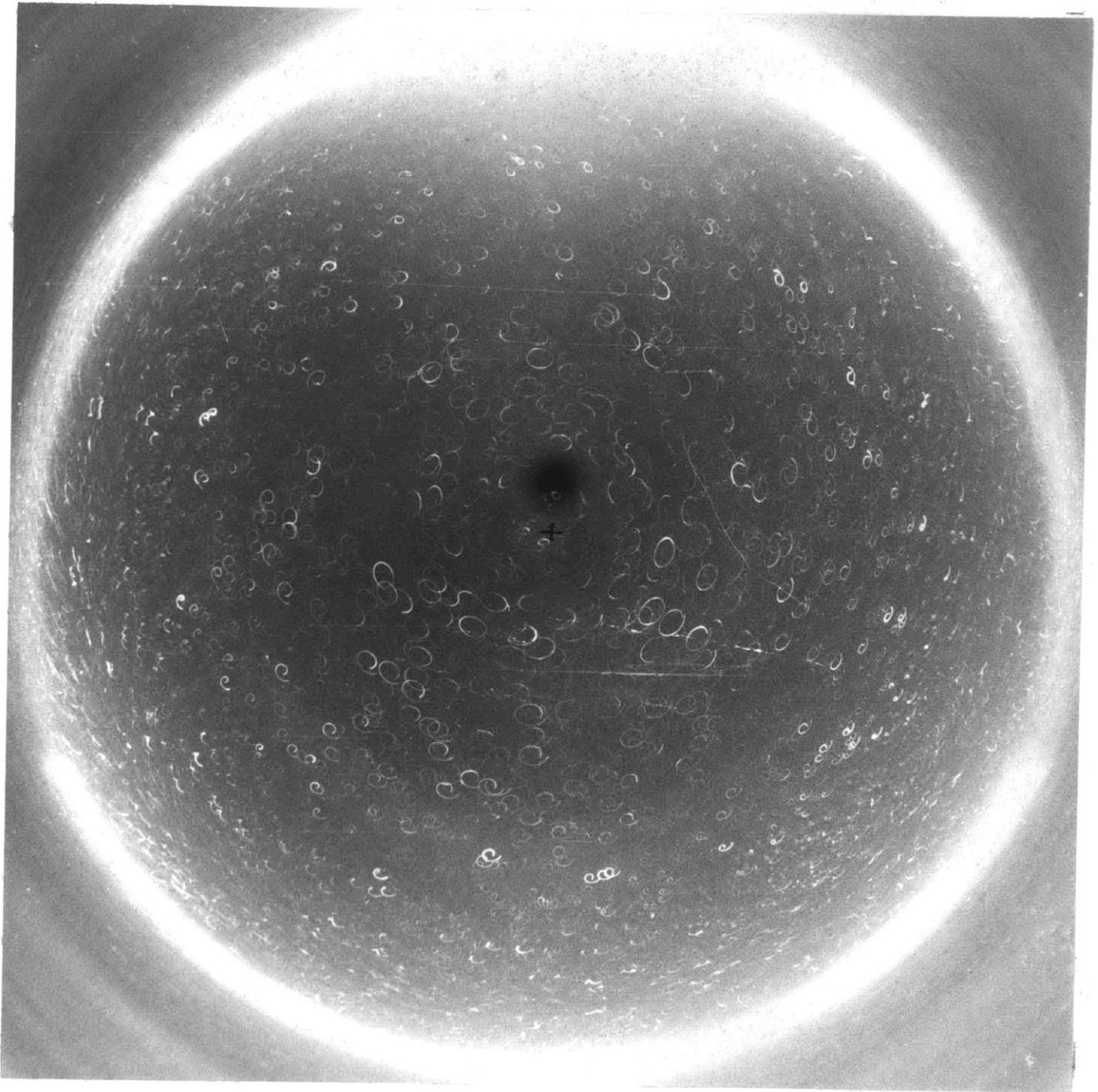time of oscillation   = T/4
light beam thickness   = 0.3 cm.

FIGURE 34

Recalling that the particle motion is counterclockwise, figures 35 and 36 clearly depict the slow counterclockwise particle drift, probably caused by the unequal particle inertia due to the basic clockwise table rotation.

Observe the small central core, large interior region and small boundary region. Notice how the wall elongates the elliptical paths near it. The amplitude of the motion increases as one moves away from the wall with the phase remaining constant. The characteristics cross near the center in figures 35 and 36.

turntable period   = 3.85 seconds
camera exposure time = 2.8 seconds
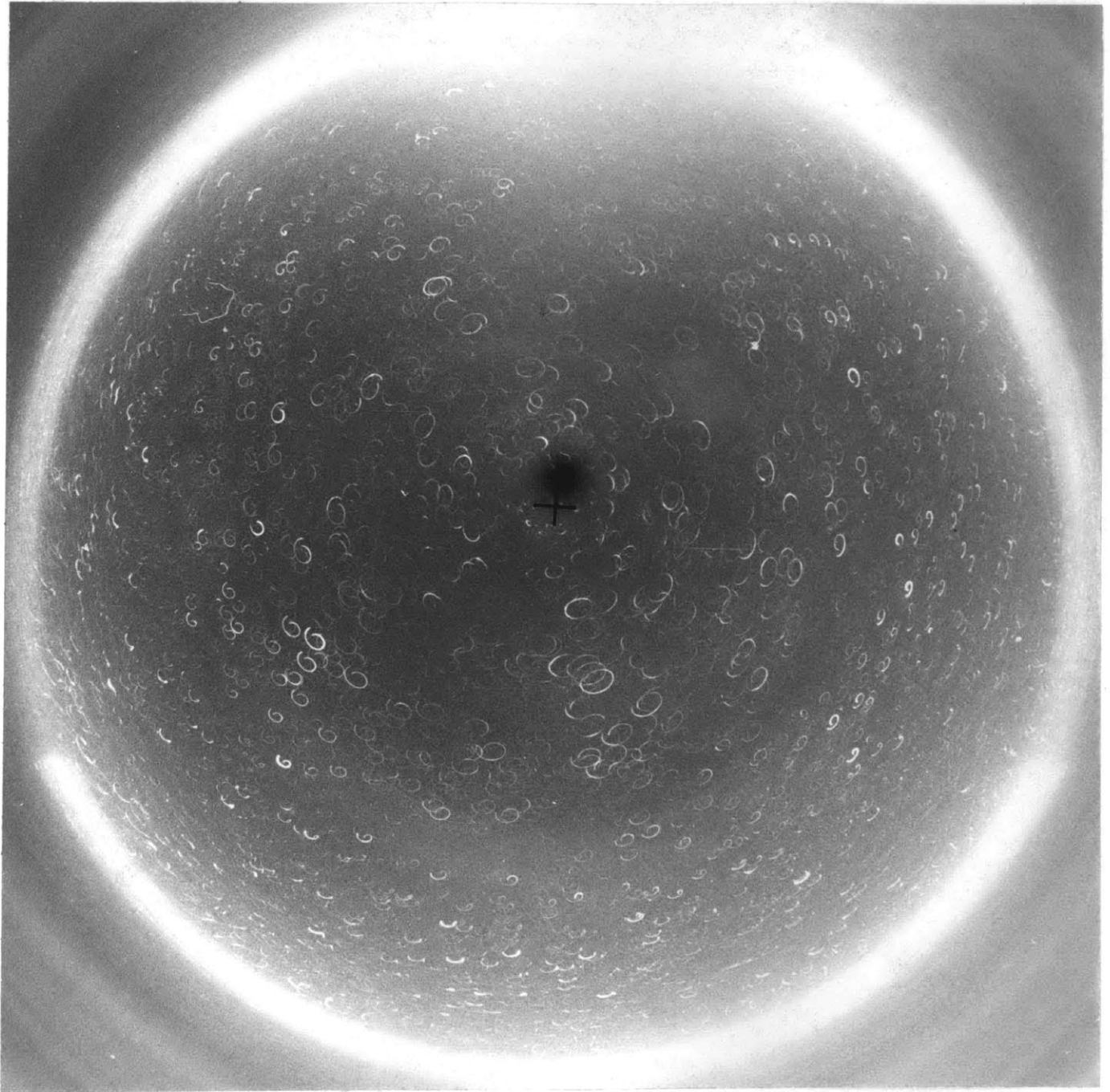time of oscillation = 3T/4
light beam thickness = 0.3 cm.

FIGURE 35

turntable period   = 3.85 seconds
camera exposure time = 2.8 seconds
time of oscillation = 3T/8
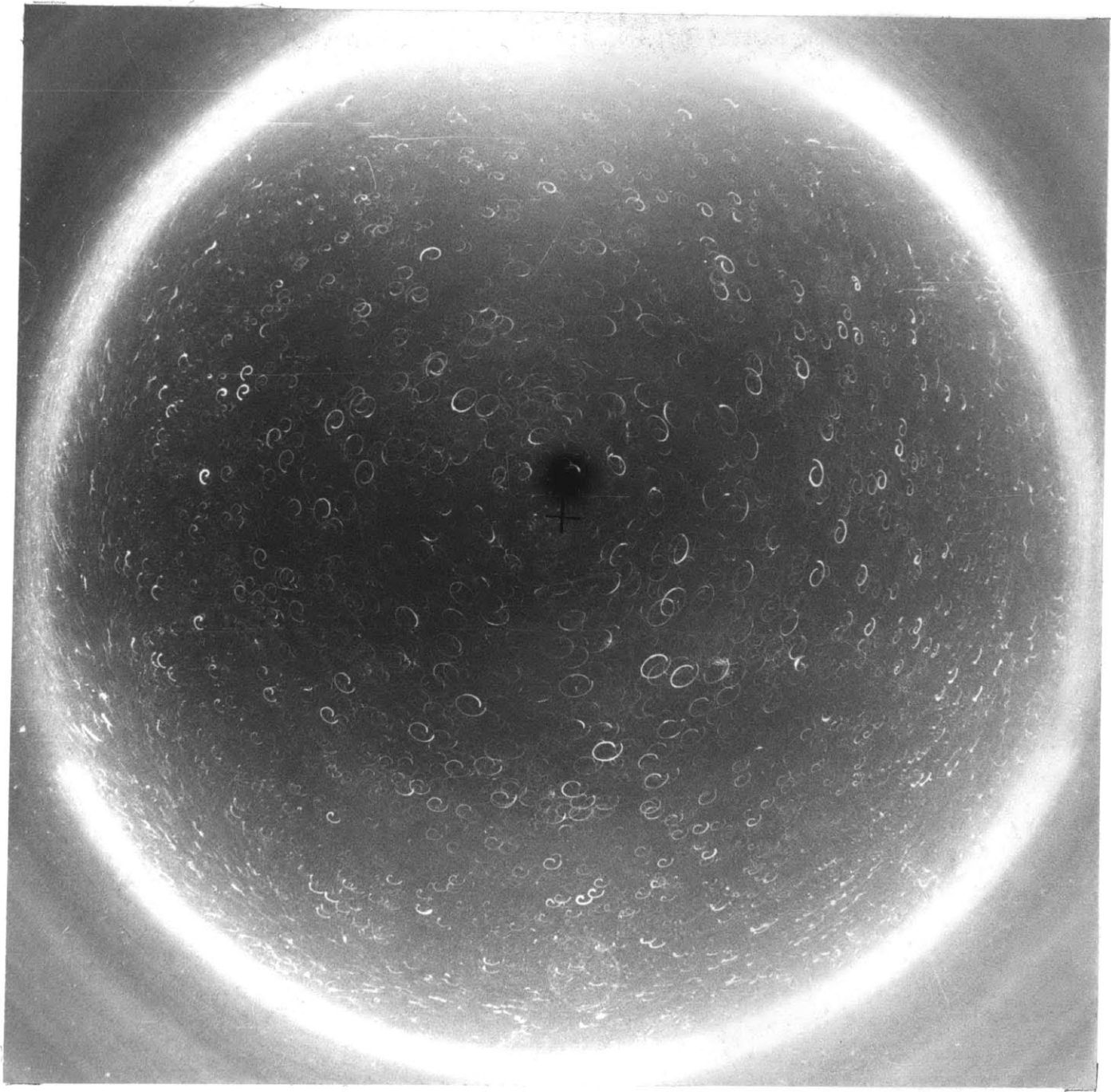light beam thickness = 0.3 cm.

FIGURE 36

In the figure 37 the lens was open for
2.8 seconds, almost one complete oscillation
period, and the picture was taken at just the
right part of the period to reveal a complete
particle revolution.

turntable period   = 3.85 seconds
camera exposure time = 2.8 seconds
time of oscillation = T/2
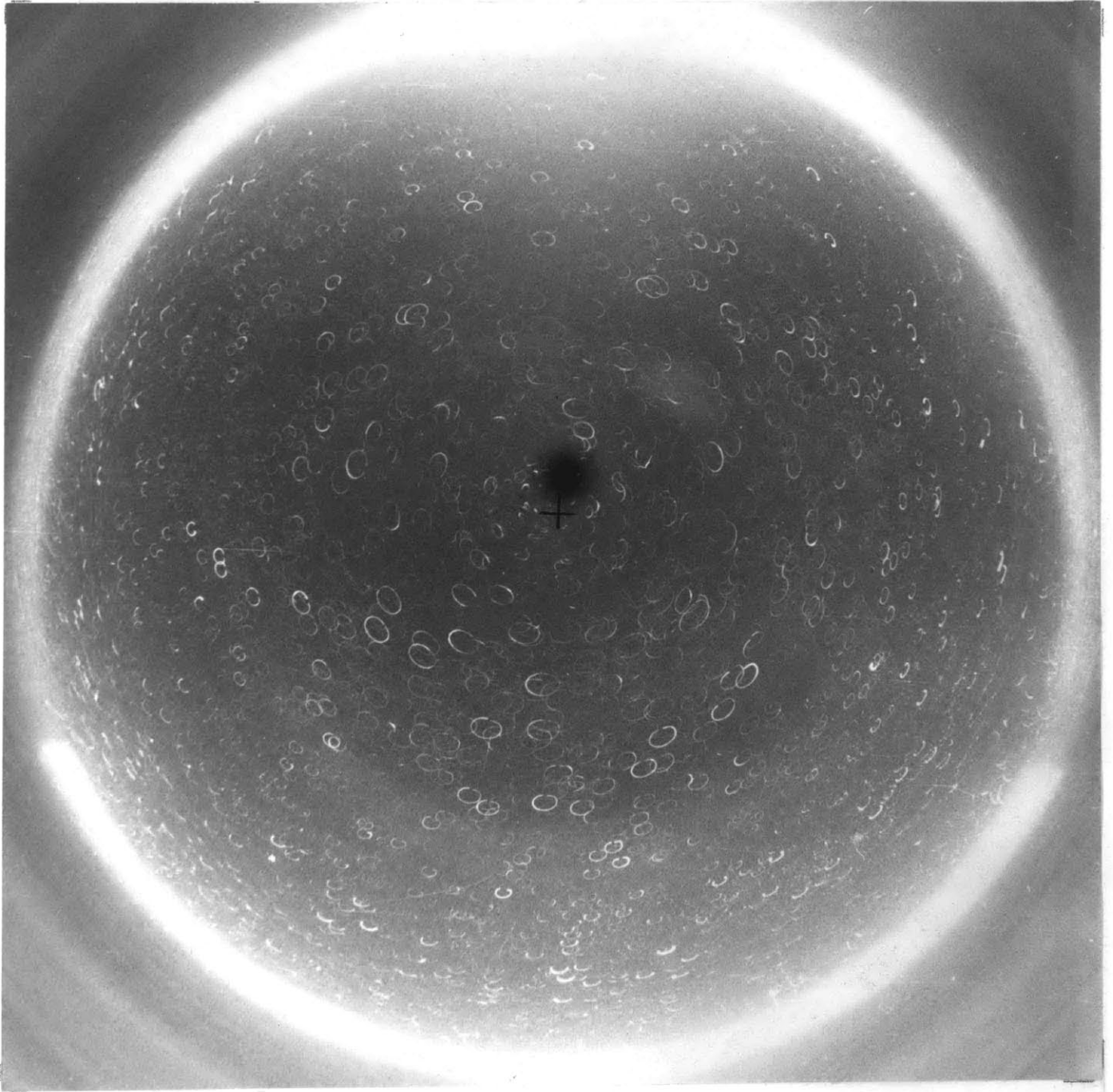light beam thickness = 0.3 cm.

FIGURE 37

Figures 38, 39, 40, display the structure
at a turntable period of 3.00 seconds. The
circle illustrates the approximate location of
the characteristic crossing. The magnitude of
the particle motion is largest near the charac-
teristics just as in the $T = 3.85$ second photo-
graphs.

turntable period   = 3.00 seconds
camera exposure time = 2.8 seconds
time of oscillation = 5T/8
light beam thickness = 0.6 cm.

FIGURE 38

Observe how the phase, constant away from
the influence of the characteristics, changes in
a smooth manner through this region, the phase on
the inside leading that on the outside by $\sim 90^\circ$
since the particle motion is counterclockwise.
Motion in the central core appears to have a small
horizontal motion.

turntable period   = 3.00 seconds
camera exposure time = 2.8 seconds
time of oscillation = 3T/4
light beam thickness = 0.6 cm.

FIGURE 39

Compare the relative magnitude of figures 38, 39, 40, with figures 23-37. Also notice the axial symmetry in all the photographs in this section.

turntable period   = 3.00 seconds
camera exposure time = 2.8 seconds
time of oscillation = 7T/8
light beam thickness = 0.3 cm.

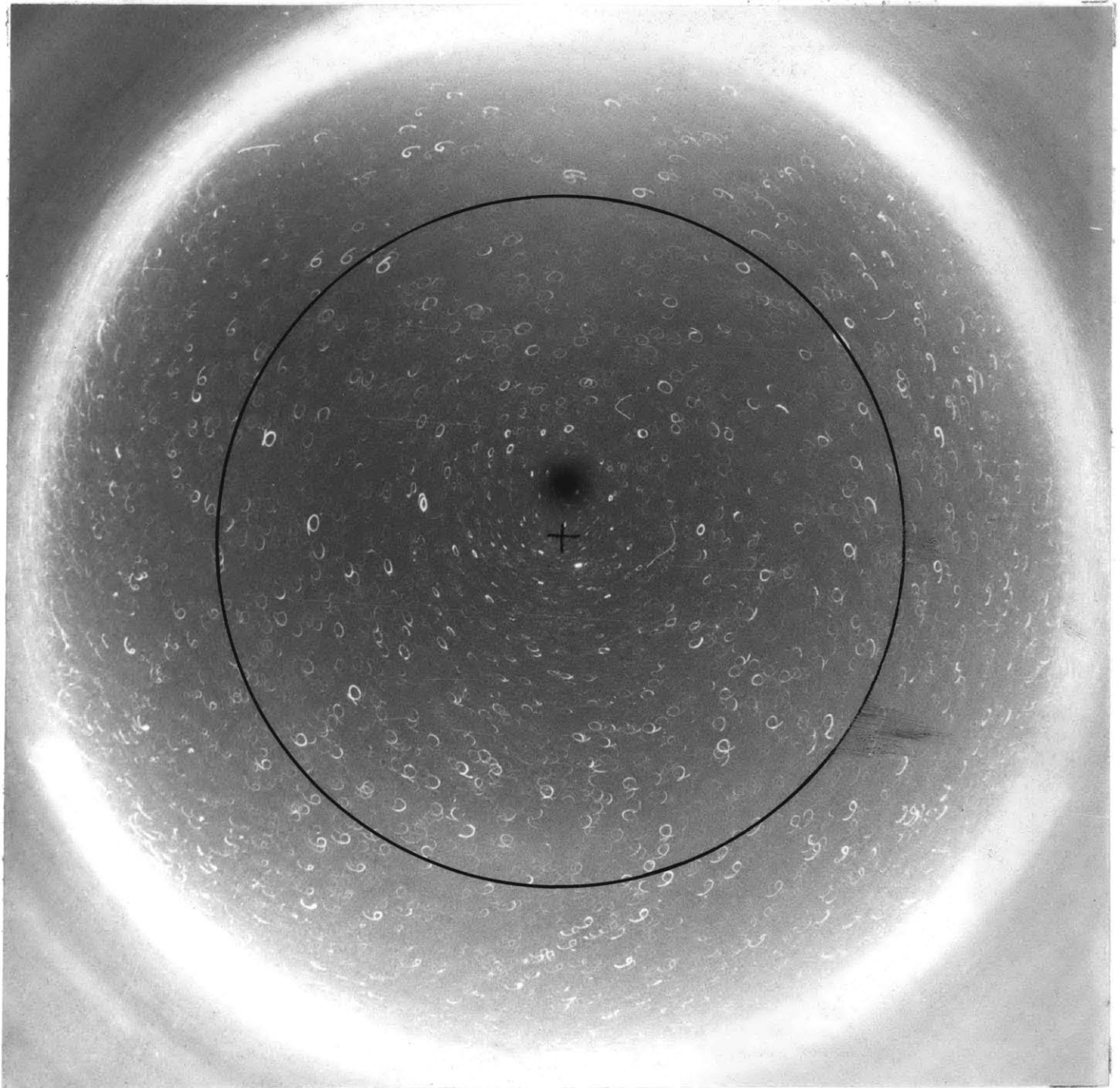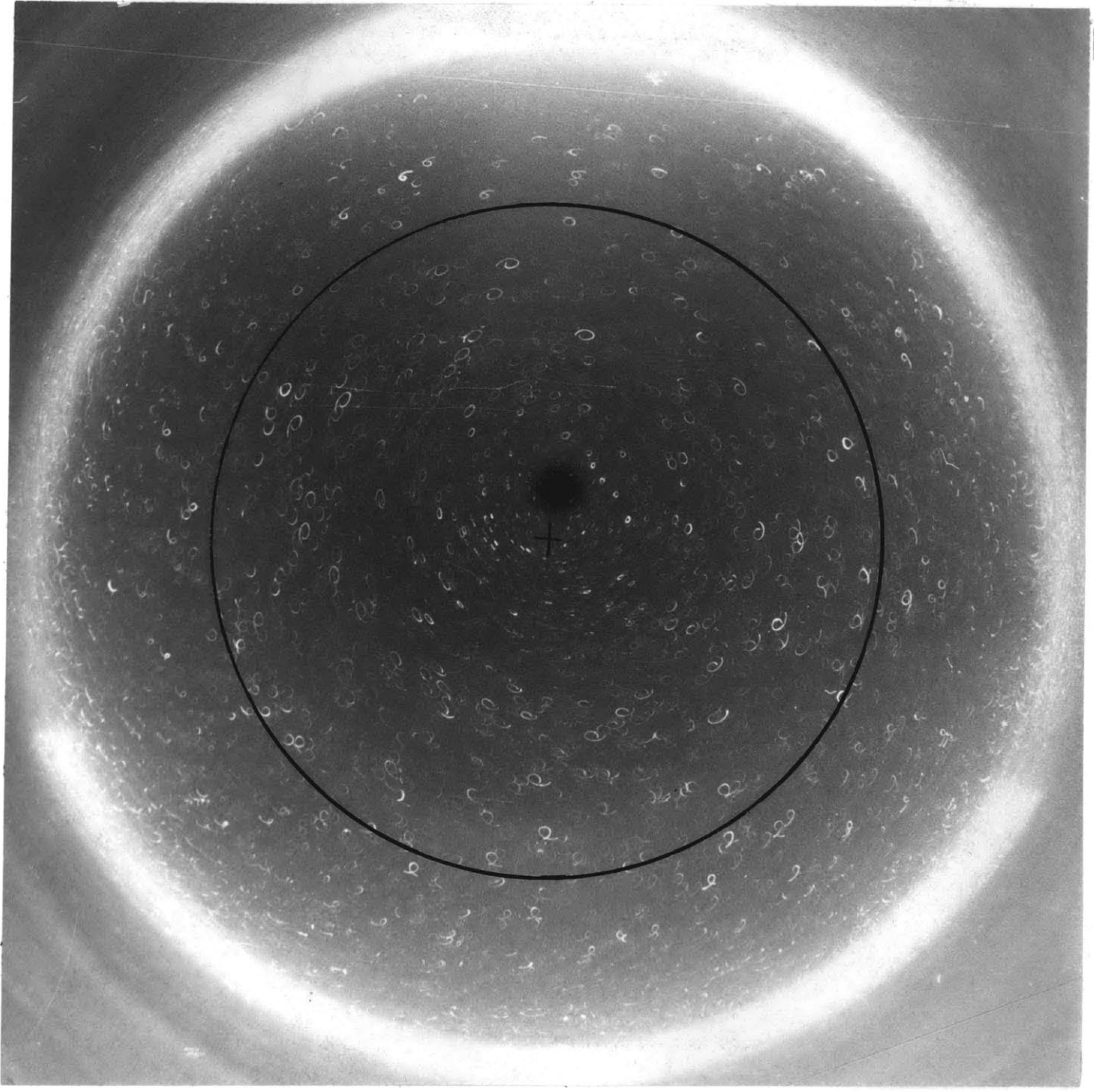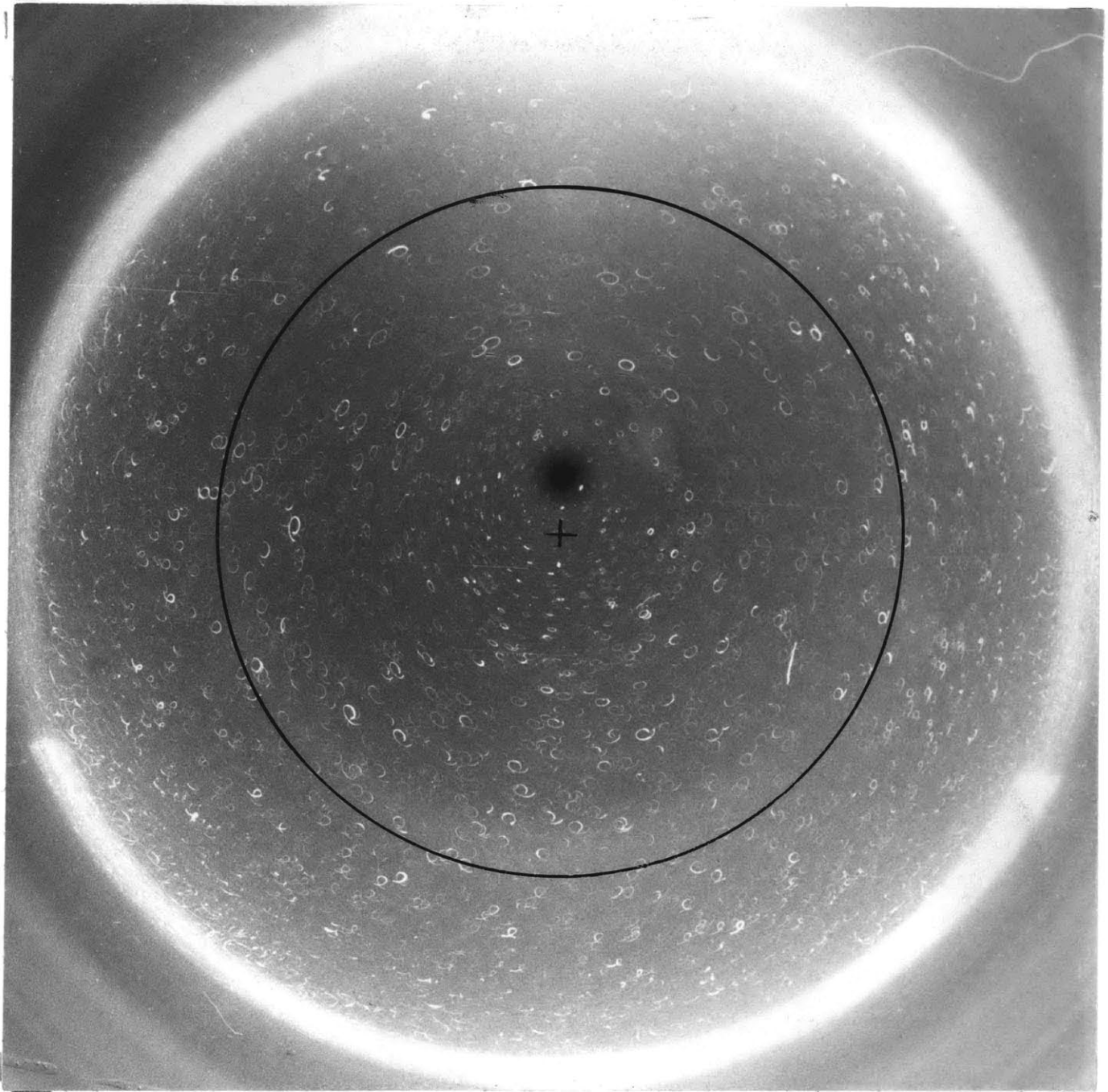FIGURE 40

5. Summary of Results

Certain axisymmetric inertial modes of oscillation of a rotating liquid cone were excited by superimposing a small harmonic perturbation, ω, on the basic turntable angular velocity. This resulted in an oscillatory fluid motion inside the cone caused by the flow separation from the upper corner with subsequent exchange of fluid between the boundary layers and the interior flow. The direction of this energy flux from the corner is given by the dispersion relation, $\Theta = \cos^{-1}\left(\frac{\omega}{2\Omega}\right)$ Θ being measured from the horizontal. The response of the fluid to different turntable rotation speeds was investigated.

The oscillatory pressure difference developed between the pole and a point on the rotation axis was measured with a pressure transducer. Similarly the oscillatory vertical velocity was measured with an axially positioned thermistor probe. A spectrum of several distinct amplitude peaks as a function of the quantity $\left(\frac{\omega}{2\Omega}\right)$ was found but these were not to be interpreted as resonance points in the cone; the location of these peaks were in good agreement with the predicted values. The shapes of the response curves from the pressure and thermistor studies were in good agreement except at fast rotation rates where unusually high pressure response was recorded by the transducer and very low vertical velocities were recorded by the thermistor probe. But for this range of turntable speeds

the characteristics are calculated to lie outside the cone $\theta > 65.8°$, $T_\tau \leq 2.3^s$, this anomalous behavior must be studied in more detail before any conclusions can be reached.

A visual study was undertaken using aluminum flakes and slit-beam lighting to obtain a detailed picture of the interior particle motion. This visual study supported the numerical data from the thermistor and pressure studies and illustrated the relationship of the characteristics to such flow parameters as velocity, phase, amplitude, boundary layer thicknesses, etc.

Finally in an attempt to obtain resonances, the cone geometry was altered by inserting a level-surfaced plug of radius 2.3 cm. in the bottom vertex of the cone so that it simulated a frustrum of a right cone. The results illustrated peaks in the response curve at the same places as in the cone study, but also revealed new peaks interspersed between these which were interpreted as resonance points due to back reflection of energy from the base of the frustrum. A further quantitative study is presently being carried out with vertical side-walls being positioned in the upper part of the cone to observe its effect on the interior flow.

It can be said that the experimental study substantiated the statements made in Greenspan's paper about inertial wave propagation in a rotating cone.

References

Aldridge, K. D. and Toomre, A. (1967), Axisymmetric inertial oscillations of a rotating sphere of fluid. To be submitted to Journal of Fluid Mechanics.

Aldridge, K. D. (1967), An experimental study of Axisymmetric inertial oscillations of a rotating liquid sphere. M.I.T. Scientific Report HRF/SR7.

Batchelor, G. K. (1967), An Introduction to Fluid Dynamics Cambridge University Press, p. 176.

Beardsley, R. C. (1967), Design and construction of a stable laboratory turntable. Laboratory Note GFD/LN5, M.I.T.

Fowlis, W. W. (1968), Techniques for the fast and precise measurement of fluid temperatures and flow speeds using multi-probe thermistor assemblies. Technical Report NO.10, Geophysical Fluid Dynamics Institute, Florida State University.

Greenspan, H. P. (1969), On the inviscid theory of rotating fluids. Studies in Applied Mathematics, M.I.T. Press. (Presently Unpublished).

Greenspan, H. P. (1968), The Theory Of Rotating Fluids. Cambridge University Press.

Landau, L. D. and Lifshitz, E. M. (1959), Fluid Mechanics. Addison-Wesley Publishing Company, pp 256-262

Phillips, O. M. (1963), Energy transfer in rotating fluids by reflection of inertial waves. The Physics Of Fluids, Vol.6, NO.4, pp 513-520

APPENDICES

A. Pressure and Phase Calibrations

Unlike the section on the thermistor response measurements which represent only relative velocity magnitudes inside the cone, the section on the pressure transducer measurements is intended to yield absolute values. To accomplish this it is first necessary to calibrate the pressure transducer.

A calibration stand was built (accuracy $\leq 3\%$) which operated on a similar principle to that of a cam. One end of a long supported shaft rested on a rotating cam while the other end supported a beaker of water which was to be raised and lowered harmonically along a vertical axis simulating the cone's oscillation. The frequency of oscillation was set equal to the cone oscillation frequency $\left(\omega = 2.22 \frac{rad}{sec} \right)$ in order to reduce electrical and mechanical losses in the system. As the beaker of water was moved harmonically a prescribed distance, the pressure was measured with a pressure probe fixed under its oscillating free surface to permit subsequent determination of absolute pressures (Aldridge 1967).

It was first necessary to carefully examine the motion of the beaker of water and to determine mathematically the importance of the various harmonics to the fundamental. Equation A-1 is the expression determined for Δh the excursions of the beaker about its mean position.

(A-1) $\Delta h = \frac{L_1}{L_2} r_0 \left\{ \epsilon \sin \omega t + \frac{1}{2} \epsilon^2 \beta^2 \sin^2 \omega t + \cdots \text{very small terms} \right.$

where $\frac{L_1}{L_2} (= 0.32)$ is the ratio of lever arm lengths, $r_0 (= 2.6 \, cm.)$

is the radius of the circular disks (the cam was made from two circular disks mounted together on a rotating shaft, the centers of which could be displaced a distance $= \epsilon r_0$, and $\beta = \frac{r_0}{L_2} =$ constant $(= 0.18)$. With the above expression, we can determine the time dependent part of the pressure in the beaker:

our equation of motion is $w_t = -\frac{1}{\rho} P_z - g$

where $w = \frac{\partial h}{\partial t}$ and $h = H + \Delta h$ is the depth of the probe below the free surface, H being its mean value. We find for the time dependent part of the pressure, ΔP_c at the probe,

$$(A-2) \qquad \Delta P_c = \rho g \, S \left(1 + \frac{H \omega^2}{g} \right) \qquad \text{to within } \pm 1\%$$

where $S = \epsilon r_0 \frac{L_1}{L_2}$ represents the amplitude of oscillation of the beaker, $\rho = $ fluid density $\left(\frac{gm}{cm^3} \right)$, $g = $ acceleration of gravity $\left(cm/sec^2 \right)$. Figure 41 presents the results of the calibration using equation (A-2). Although the calibration line is not horizontal which would indicate linearity of the transducer it is still small enough that for the range of pressures in the cone $\left(\sim 0.5 \text{ to} \sim 7.5 \; mm \, H_2 0 \right)$ we can choose one value as a calibration constant $\left(E = 176.0 \frac{\mu V}{mm \, H_2 0} \right)$. Since the pressure signals had to be analyzed in a correlator, an amplitude calibration had to be made on this piece of equipment. This calibration consisted of sending two known sinusoidal signals through the correlator and monitoring their amplitude and phase. The result was a calibration constant $C = 5.74 \pm .04 \frac{\mu V}{\text{unit of meas.}}$ Thus if our pressure signals had an amplitude of X units, this
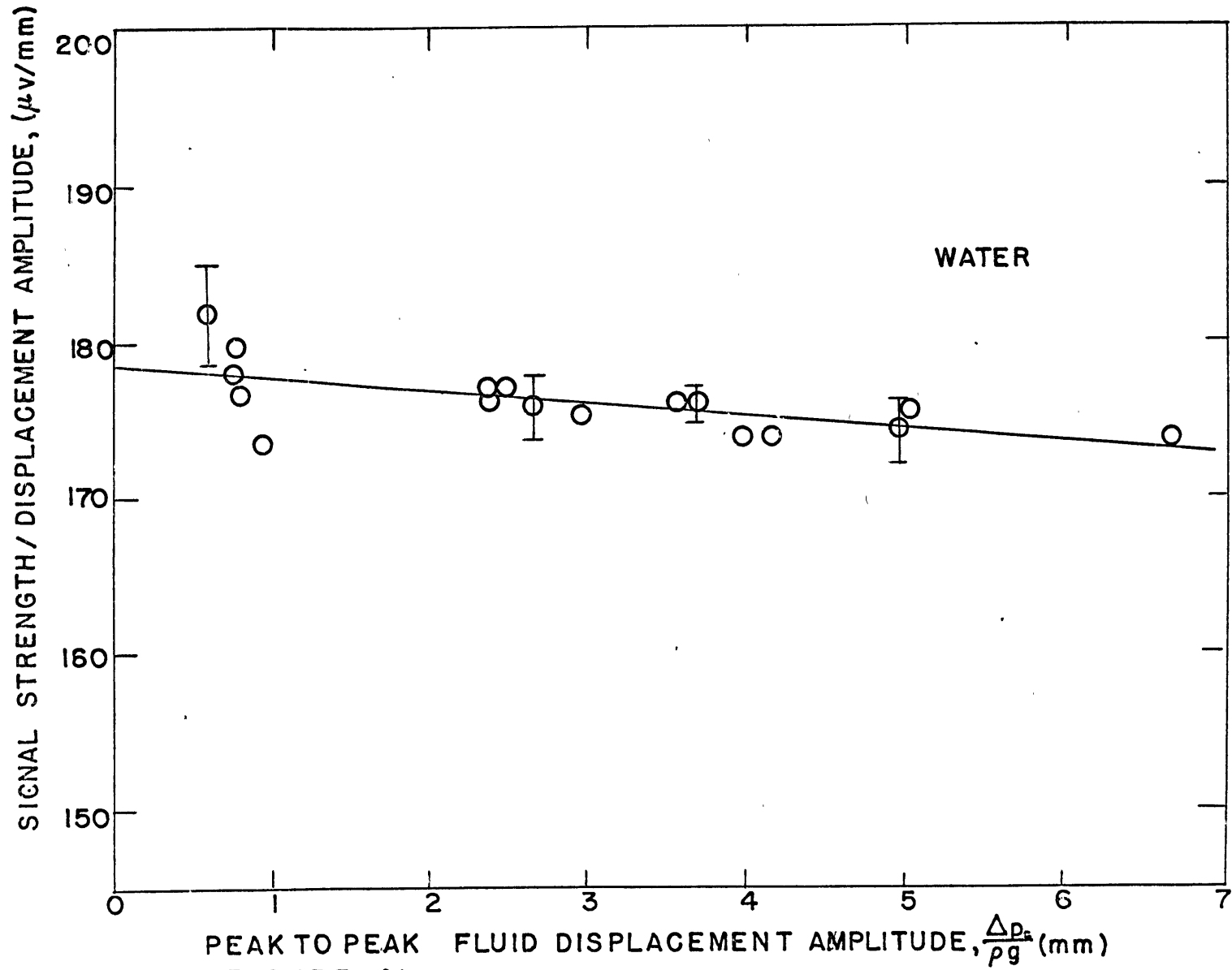
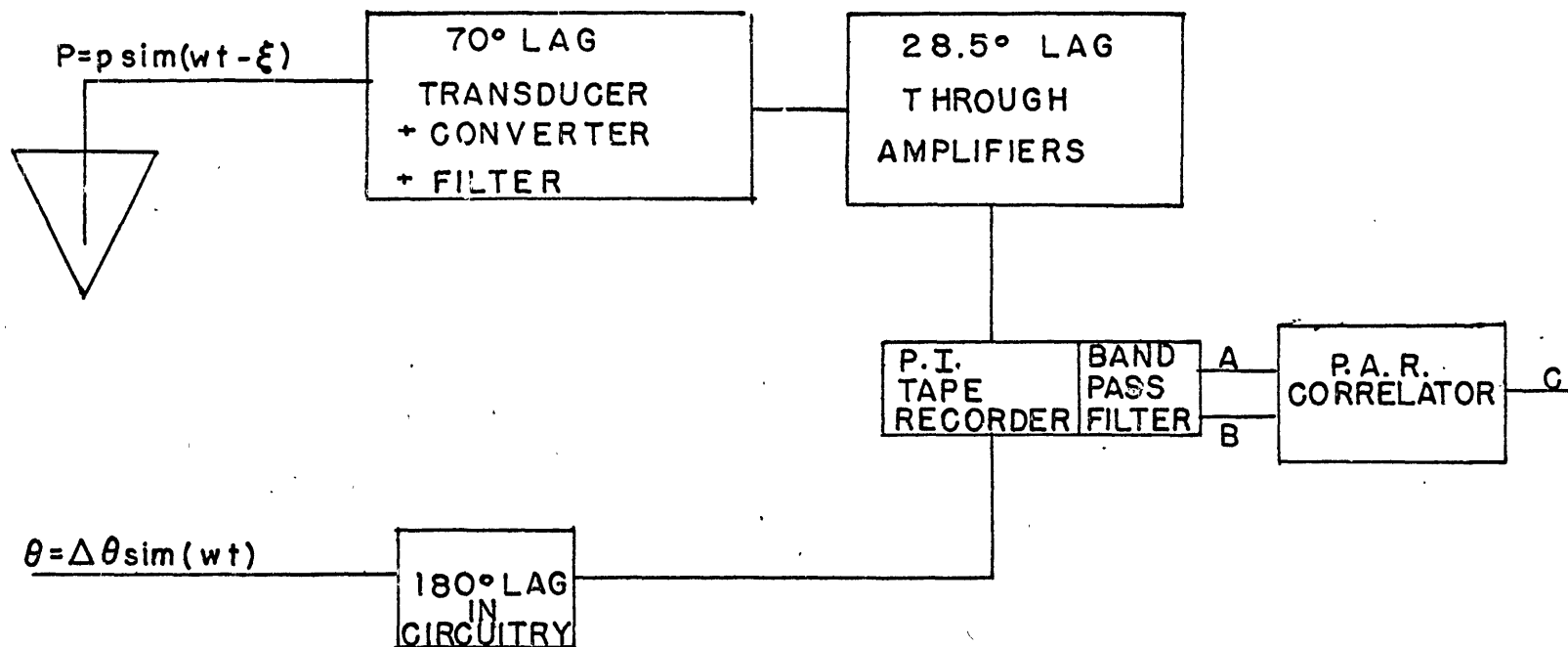PRESSURE TRANSDUCER CALIBRATION

WATER

FIGURE 41

would correspond to an absolute pressure ΔP_A

$$\Delta P_A = \rho g \times \frac{c}{E}$$

It is $\frac{\Delta P_A}{\rho g}$ versus T_T turntable period which is plotted in
figures 16 and 17.

Since the photographs indicated a smoothly changing part-
icle phase of $\sim 90^\circ$ across the characteristic region, it was
felt that this effect might reveal itself in a phase sensitive
device such as the P.A.R. correlator. This is equivalent to
asking the question whether the phase is dependent in any way
on the parameter $\left(\frac{\omega}{2\pi}\right)$, or whether the phase remains a constant.
It is expected that as the cone oscillates the fluid in the
boundary layers along the walls will not stay in phase with it
but that there will be some lag. Also it takes a finite time
for the energy to propagate from the upper corner to the sens-
ing device mounted on the axis of the cone. It is thought
that these latter two effects will be the major cause of phase
lag (or lead). Figure 42 is a schematic of the phase calibration
performed on the experimental apparatus, with ξ equal to the
phase lag between the pressure signal and the corresponding
part of the cone oscillation. The π-phase lag in circuitry
refers to the potentiometer signal going negative for a clock-
wise cone oscillation. $\Delta = \pi - \Theta_{meas}$ refers to the fact that
it was not Δ that was measured off the correlator output but
rather Θ_{meas} . Therefore our equation to calculate the phase

$P = p \sin(wt - \xi)$

70° LAG
TRANSDUCER
+ CONVERTER
+ FILTER

28.5° LAG
THROUGH
AMPLIFIERS

P.I.
TAPE
RECORDER

BAND
PASS
FILTER

A

B

P.A.R.
CORRELATOR

C

$\theta = \Delta\theta \sin(wt)$

180° LAG
IN
CIRCUITRY

ξ = LAG OF PRESSURE SIGNAL BEHIND CONE POSITION

$A = p \sin(wt - 70° - 28.5° -$

$B = \Delta\theta \sin(wt - \pi)$

$C = \dfrac{p\Delta\theta}{2} \cos(wt + \Delta)$

$\Delta = 70° + 28.5° + \xi - \pi = \pi - \theta$ meas.

FIGURE 42

lag in degrees is

$$\xi \, (degrees) = 3.27 \left(79.9 - \Theta_{meas.}\right)$$

Figures 43 and 44 are plots of ξ versus turntable period for the cone and frustrum geometry. The variation in ξ is about 100 degrees. Although the results of phase lag are not as conclusive as the absolute pressure readings, one can draw some information from these curves. Both curves appear to have a similar shape with peaks and valleys occurring at similar turntable periods, also the magnitudes of the phase in degrees are equivalent. If one refers to figures 16 and 17 it appears that when the characteristics lie inside the rotating body $(T_T \leq 2.4$ seconds$)$ a large pressure response corresponds to a small phase lag and vice versa, although this statement is not fully justified as the peaks and valleys of the pressure and phase curves do not line up exactly. The exception being when the characteristics lie outside the rotating body, in this case an unusually large pressure response corresponds to a large phase lag.
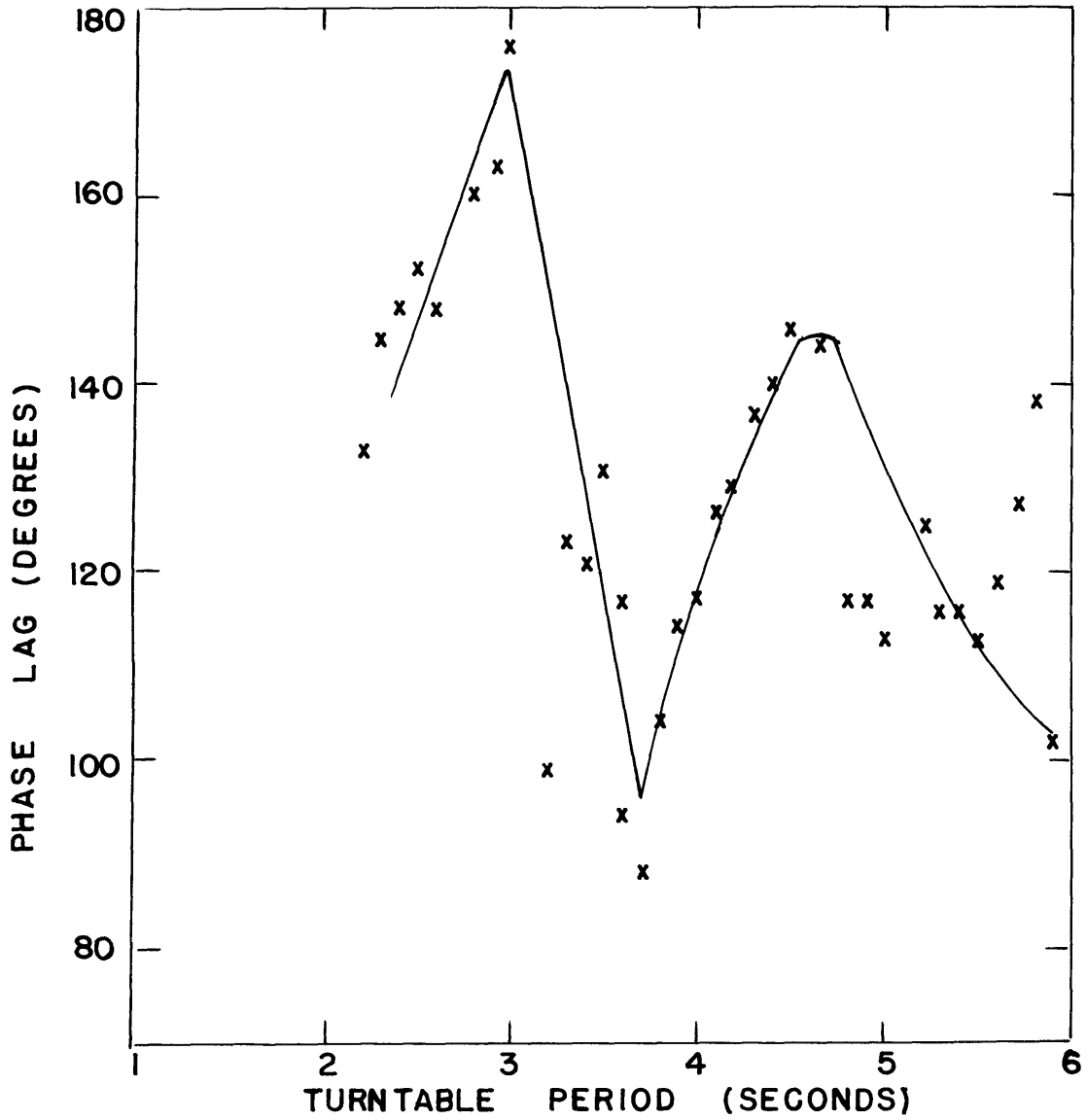
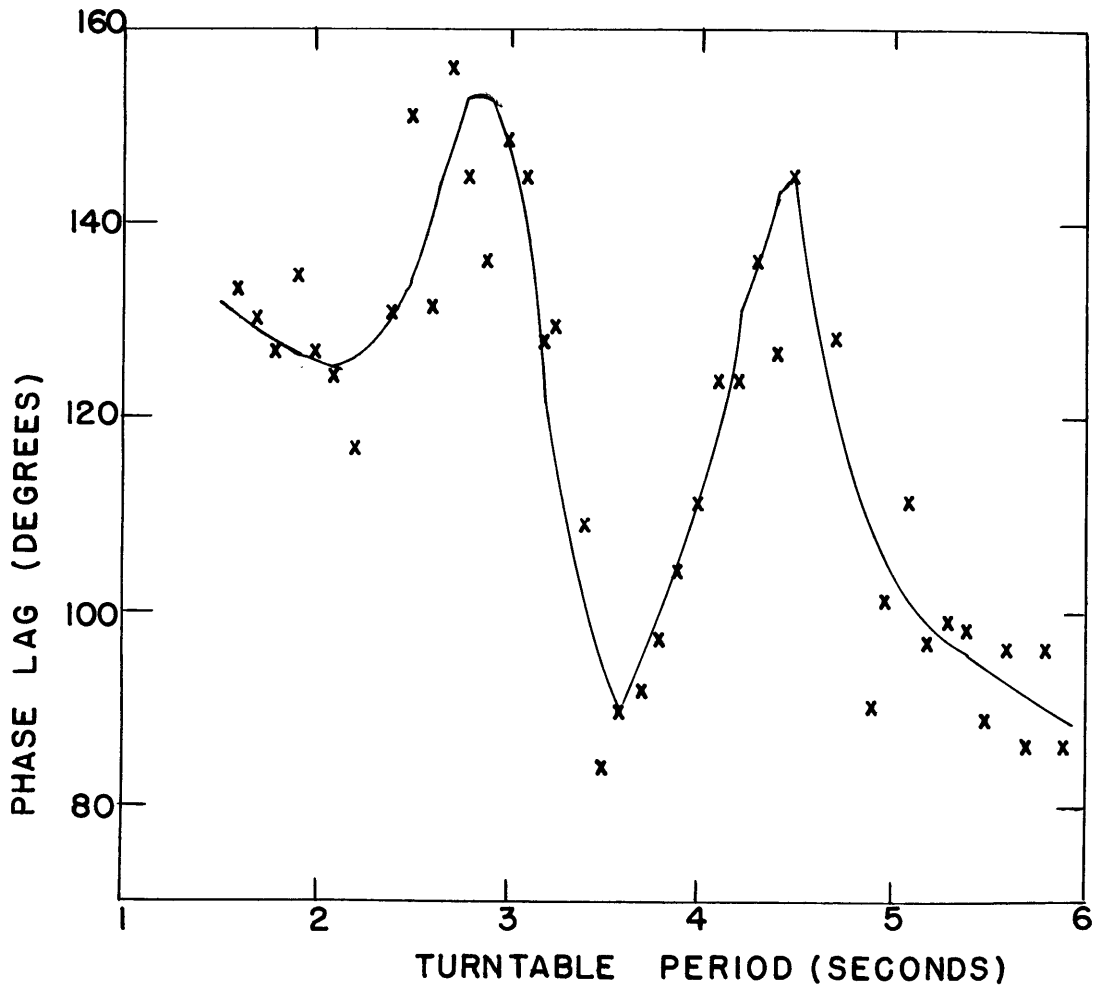PHASE CALIBRATION - FRUSTRUM

FIGURE 43

PHASE CALIBRATION - CONE

FIGURE 44

B. Reflection of Characteristics

$\tilde{C}_g$ is the direction of energy propagation given by the dispersion relation $\Theta = \cos^{-1}\left(\frac{\omega}{2\Omega}\right)$, Θ being measured from the horizontal, figure 45; whence D_1, the depth of the first axial crossing of the characteristics is at once determined from elementary trigonometry

$$D_1 = r_0 \tan\Theta = r_0 \frac{\sqrt{1-\cos^2\Theta}}{\cos\Theta}$$

In an X-Y co-ordinate system, with the cone on its side as illustrated in figure 46, the general equation for $\tilde{C}_g$ is given by

$$y = mx + b$$

(B-1)
$$y = -\frac{1}{\tan\Theta}x + 2r_0$$

the equation of the cone wall is:

(B-2)
$$y = x\tan\beta$$

setting (B-1) and (B-2) equal to each other to determine their point of intersection (X_0, Y_c), yields

(B-3)
$$X_0 = \frac{2r_0}{\tan\beta + \frac{1}{\tan\Theta}}$$

at this point the distance to the central axis of the cone is,

$$r_1 = r_0 - y_c = r_0 - X_0\tan\beta$$

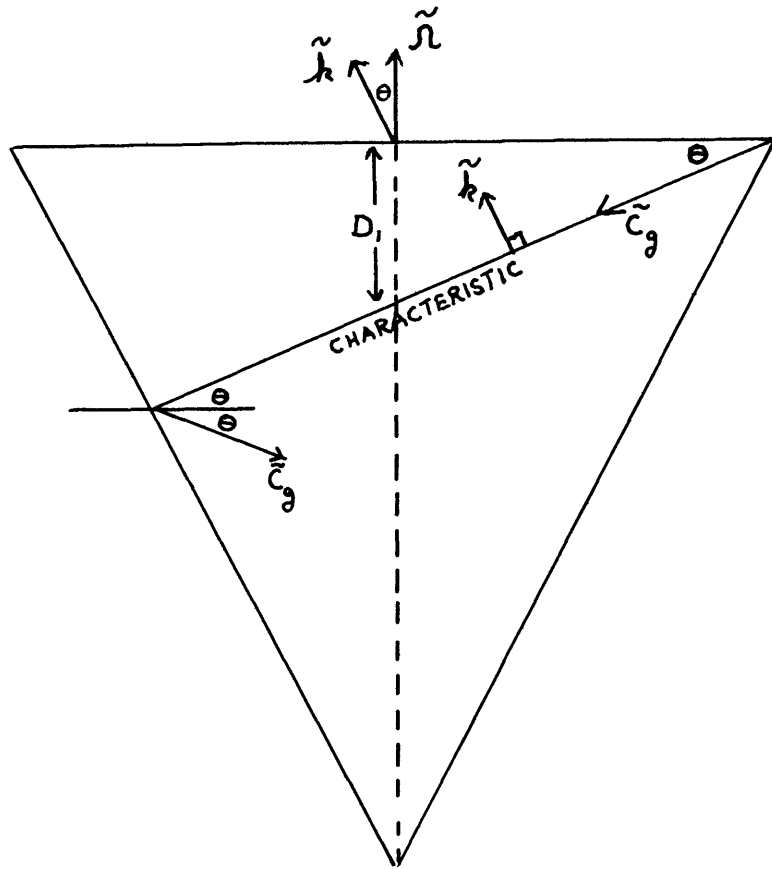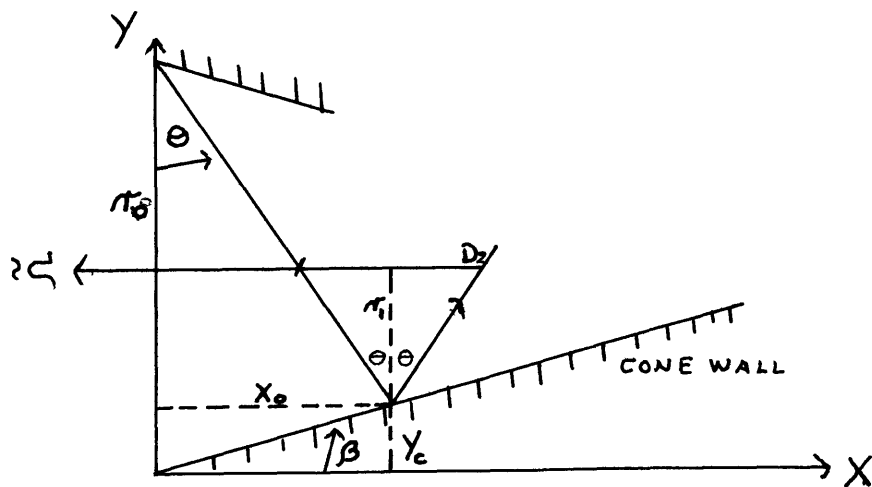from this value r_1, we can determine D_2, the 2nd axial crossing

FIGURE 45

FIGURE 46

point of the characteristic emanating from the corner at angle θ :

$$D_2 = x_0 + \tan\theta \left(r_0 - x_0 \tan\theta \right)$$

by similar triangles, using figure 47,

$$\frac{d_4}{d_3} = \frac{d_3}{d_2} = \frac{d_2}{d_1}$$

and

$$\frac{d_2}{d_1} = \frac{r_1}{r_0} = 1 - \frac{x_0}{r_0}\tan\beta$$

but from equation (B-3)

$$\frac{x_0}{r_0} = \frac{2\tan\theta}{\tan\beta\tan\theta + 1}$$

so

$$\frac{d_2}{d_1} = 1 - \frac{2\tan\theta\tan\beta}{\tan\beta\tan\theta + 1}$$

set

$$\sigma = \tan\beta\tan\theta = \frac{\tan\beta\left[1 - \left(\frac{\omega}{2\Omega}\right)^2\right]^{1/2}}{\left(\frac{\omega}{2\Omega}\right)}$$

rewriting this,

$$\sigma = \tan\beta\sqrt{\left(\frac{2\Omega}{\omega}\right)^2 - 1}$$

to get

$$\frac{d_2}{d_1} = \frac{1 - \sigma}{1 + \sigma}$$

Now using the above equations we can calculate the various axial crossing points of a characteristic as it proceeds toward the vertex of the cone.

1st crossing $D_1 = d_1$ ———————————→ $d_1(1)$

2nd crossing $D_2 = d_1 + 2d_2$ ———————————→ $d_1\left(1 + 2\frac{d_2}{d_1}\right)$

3rd crossing $D_3 = d_1 + 2d_2 + 2d_3$ ———————————→ $d_1\left(1 + 2\frac{d_2}{d_1} + 2\left(\frac{d_2}{d_1}\right)^2\right)$

4th crossing $D_4 = d_1 + 2d_2 + 2d_3 + 2d_4$ ——————→ $d_1\left(1 + 2\frac{d_2}{d_1} + 2\left(\frac{d_2}{d_1}\right)^2 + 2\left(\frac{d_2}{d_1}\right)^3\right)$

and the general expression for the nth axial cross is

(B-4)   nth crossing $D_m = d_1 \left(1 + 2 \frac{d_2}{d_1} + 2 \left(\frac{d_2}{d_1}\right)^2 + \cdots + 2 \left(\frac{d_2}{d_1}\right)^{m-1} \right)$

Below is developed a general equation to calculate the radial position of the characteristics on the photographs in the visual study section of this text, see figure 48.

the radial position of the characteristics in the cone, is given by $r_c = r_0 - \frac{h}{\tan\theta}$ where h = distance of picture from the top of cone

the radius of the cone at depth h is

r_T = 10.59 tan 24.16° or equivalently = $r_0 - h\tan\beta$

their ratio, f, which can be used in analyzing the actual photographs is

(B-5) $f = \frac{r_c}{r_T} = \frac{r_0 - \frac{h}{\tan\theta}}{r_0 - h\tan\beta} = \frac{r_0 - \frac{h}{\tan\theta}}{10.59\ \tan 24.16°}$
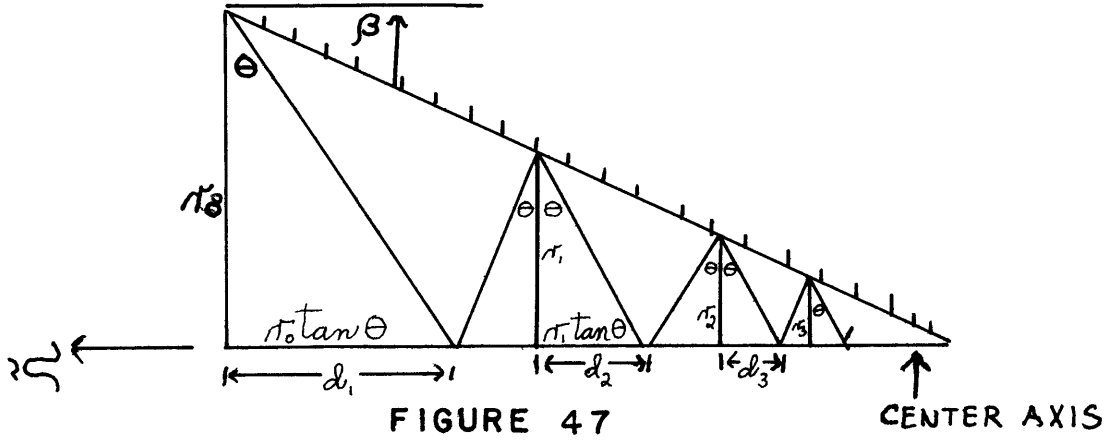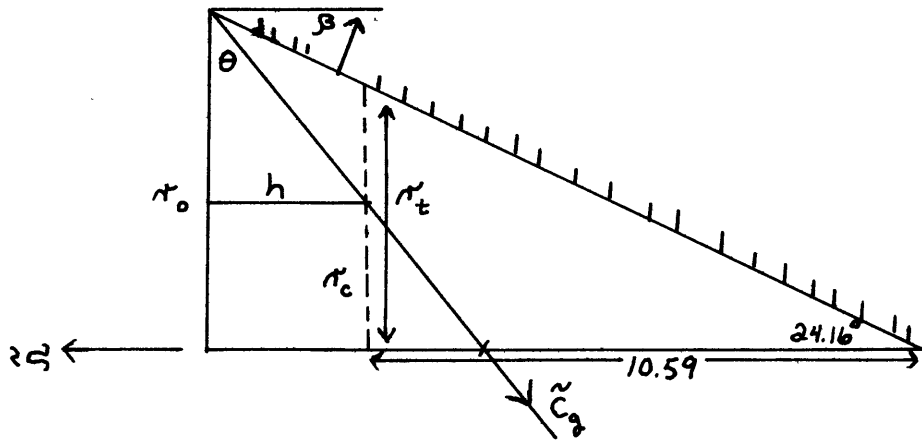
FIGURE 47

FIGURE 48

C. <u>Computer Program for Calculation of Axial Crossing Points of Characteristics</u>

```
      DIMENSION A(20),AA(20),TO(20),DO(20),DDO(20),
      SIGMA(20),X1(20),X2(20),X3(20)
      TB = .44858
      RO =  9.049
      READ (5,100) K
100   FORMAT (I3)
      READ (5,101) (A(I), I=1,K)
101   FORMAT (12F6.4/F6.4)
      DO900 I=1,K
      AA(I)=1./A(I)
      TO(I)=SQRT(AA(I)**2-1.)
      SIGMA(I) = TB *TO(I)
      DDO(I) = (1.-SIGMA(I)/(1.+SIGMA(I))
      DO(I)=RO*TO(I)
      X1(I) = DO(I)*(1.+2.DDO(I))
      X2(I) = X1(I) + DO(I)*2.*DDO(I)**2
      X3(I) = X2(I) + DO(I)*2.*DDO(I)**3
900   CONTINUE
      WRITE(6,200)
200   FORMAT(1H1,6X,4HA(I),8X,2HDO,8X,2HX1,8X,2HX2,8X,2HX3)
C
C WRITE RESULTS
C
      DO 901 I=1,K
      WRITE (6,201) A(I),DO(I),X1(I),X2(I),X3(I)
201   FORMAT (4X,5F10.4)
901   CONTINUE
      END
```

BIOGRAPHICAL NOTE

The author was born on 14 February 1945 in Boston, Massachusetts. He attended Boston Latin High School and entered college in the Department of Physics at Northeastern University in September 1962. He graduated "cum laude" in June 1967 with the degree of Bachelor of Arts in Physics. While at Northeastern University he distinguished himself as secretary of the Northeastern Chapter of the American Institute of Physics. During the time span April 1963 through August 1967 Mr. Carter worked part-time at Avco Research Laboratory in the field of atmospheric and re-entry physics culminating his endeavors with the publication of several government research papers on re-entry vehicle performance. His most recent work at Avco was accomplished while holding a position as assistant scientist on their scientific staff. In the fall of 1967, he extended his fields of study to Inner Space by enrolling at M.I.T. as a graduate student in the Department of Geology and Geophysics with especial interest in physical oceanography and fluid mechanics.